Inorganic Chemistry

pubs.acs.org/IC

Article

Dinuclear Organoruthenium Complex for Mitochondria-Targeted Near-Infrared Imaging and Anticancer Therapy to Overcome Platinum Resistance

Jiaoyang Wang, Yufei Zhang, Yifan Li, Enbo Li, Wenjing Ye,* and Jie Pan*

Cite This: *Inorg. Chem.* 2022, 61, 8267−8282

Read Online

ACCESS | Metrics & More | Article Recommendations | Supporting Information

ABSTRACT: New mononuclear and dinuclear Ru(II) coordination compounds with the 2,7-bisbenzoimidazolyl-naphthyridine ligand have been synthesized and characterized by UV−vis, NMR, and MALDI-TOF. The molecular structures for Ru(II) compounds were determined by single-crystal X-ray diffraction. With the expansion of ligand π-conjugation and the increase in the complexed Ru number, the maximum emission wavelength red-shifted from 696 to 786 nm. The binding mode between complexes and DNA was predicted by molecular docking, which is intercalations and $\pi-\pi$ stacking interactions with the surrounding bases. The intercalation mode of DNA binding was then determined by DNA titration and ethidium bromide (EB) displacement experiments. The antigrowth effects of complexes **RuY**, **RuY1**, and **RuY2** were tested in HaCat (normal cells), HeLa (cervical cancer), A549 (lung cancer), and A549/DDP (cisplatin-resistant lung cancer) through the MTT assay. The dinuclear complex **RuY2** was superior to mononuclear complexes and cisplatin in the cisplatin-resistant cell line. Confocal imaging proved that the subcellular localization of Ru(II) complexes was mitochondria; moreover, apoptosis was detected by flow cytometry. All three complexes showed a dose-dependent manner in all four cell lines. All Ru(II) complexes were found to have reactive oxygen species (ROS). The finding indicated that these Ru(II) complexes caused cell death by both DNA disruption and ROS. This study helps to explore the potential of the polynuclear Ru(II) complexes for the combination of NIR imaging and Pt-resistant cancer therapy.

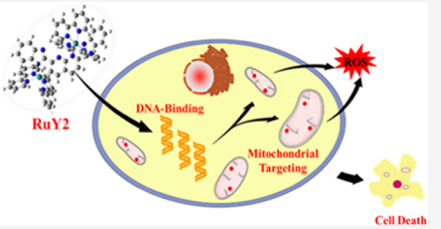

INTRODUCTION

Platinum-based anticancer drugs have been used for chemotherapy for almost 40 years due to its effective toxicity toward cancer cells.[1] Some classic Pt drugs have been developed in clinics and used worldwide such as cisplatin, carboplatin, and oxaliplatin.[2−4] However, some side effects have significantly influenced their worldwide use due to drug resistance and toxicity without selectivity.[5] To eliminate such side effects and explore the novel mechanisms of cell death, new anticancer drug candidates are in demand urgently.

Under this circumstance, transition metals such as ruthenium, iridium, and osmium are of interest due to their comparative lower toxicity, better selectivity, and novel mechanism for causing cell death. For example, these new mechanisms include DNA binding, inhibition of the activity of the proteins, or catalytic hydride transfer reactions in cells.[6−8] Moreover, after the metal is complexed with π-conjugated auxiliary ligands such as arene,[9] polypyridine,[10] 1,10-phenanthroline,[11] and their derivatives, with the modification of ligands, novel transition metal complexes can lead to a significant change in luminescence properties and anticancer efficacy. Among these transition metal complexes, Ru(II) complexes were attractive due to their special photophysical properties and DNA binding mechanism for anticancer therapy.[12] Some Ru(II) complexes have been used in clinical trials such as **NAMI-A**,[13] **KP1019**,[14] and **(N)KP1339**[15] (Figure 1). However, these above-mentioned probes did not reach the near-infrared (NIR) region, which was not suitable for NIR imaging. NIR imaging has several advantages such as minimum photodamage to biological tissue, deep penetration depth, less light scattering, and fast and cheap technique.[16−21] We believe that combining imaging techniques with the anticancer properties of Ru complexes will lead to better tumor therapeutics. Therefore, the design of ligands is very important. With the design of π-conjugated ligands, the charge transfer of metals to ligands can extend the emission range to the NIR region with relatively longer wavelengths.

Polynuclear complexes provide a novel design as anticancer agents, which may display additional advantages over mononuclear counterparts such as longer emission wavelength, improved anticancer efficacy, and lower toxicities. Subtle examples are $[(\text{arene})_2\text{Ru}_2\text{L}]^{2+}$,[5] **BBR3464**,[22] and Ru(η^6-*p*-cymene) complexes[23,24] (Figure 1). However, there are only a few examples of polynuclear ruthenium complexes in the reported results, and even fewer of them reached the near-

Received: March 4, 2022
Published: May 18, 2022

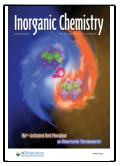

https://doi.org/10.1021/acs.inorgchem.2c00714
Inorg. Chem. 2022, 61, 8267−8282

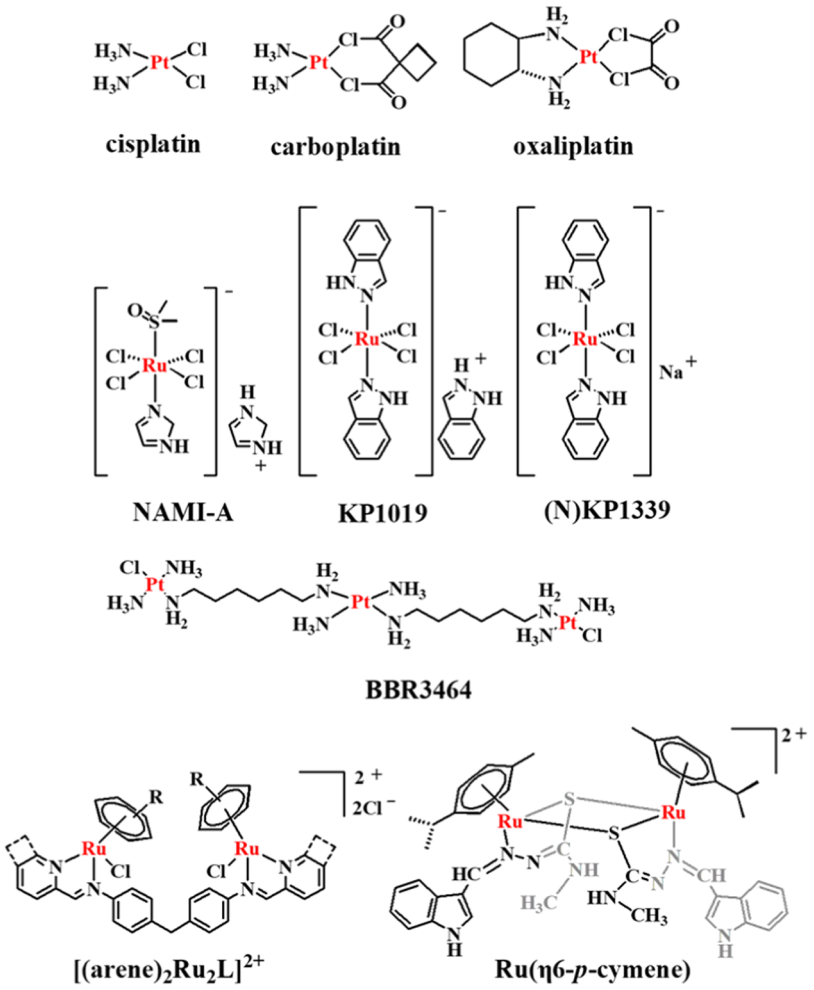

Figure 1. Representative anticancer platinum(IV) and ruthenium(II) complexes.

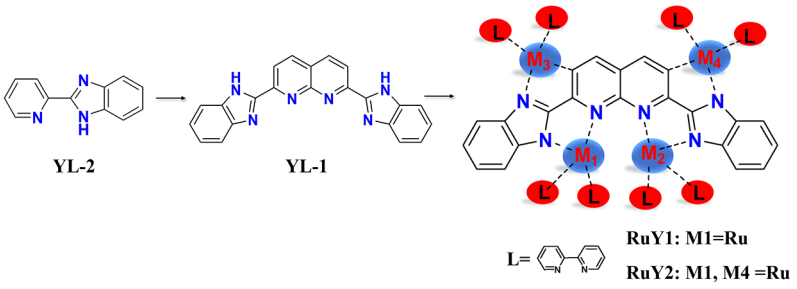

Figure 2. Design of a novel ligand for a polynuclear anticancer drug.

infrared region (650−900 nm).[25−27] Therefore, well-designed polynuclear ruthenium needs to be developed, and more extensive studies are required.

In our and other groups' previous studies,[28−32] the pyridiyl-benzimidazole ligand (**YL-2**) had sufficient coordination sites that provided possibilities for complexation to metal and DNA binding and a large π-conjugated system for red-shifted emission wavelengths. Based on the pyridiyl-benzimidazole moiety, herein, a newly designed ligand, 2,7-bisbenzoimidazolyl-naphthyridine (**YL-1**), is constructed by two benzimidazoles conjugated with a naphthyridine moiety. Compared to the pyridiyl-benzimidazole ligand (**YL-2**), **YL-1** had an expanded π-conjugated system and more binding sites for polynuclear complexation (**M1** to **M4**), as shown in Figure 2. In the following synthetic work, we first complexed a Ru at the **M1** position to synthesize a mononuclear **RuY1** complex. Then, *t*BuOK was used as a strong base for the removal of hydrogen chloride. The second Ru was then complexed at the **M4** position instead of **M2**, which may be due to the steric hindrance effect. For other vacant coordination sites of Ru, we used bipyridine as the ligand for complexation, which resulted in **RuY2** (Figure 2). The molecular structures for Ru(II) compounds were determined by single-crystal X-ray diffraction. Photophysical studies, docking analysis, CT-DNA binding mode, antigrowth effect, ROS generation, cell cycle capture, confocal imaging, and apoptosis studies have been done. Through these tests, we hoped that our designed dinuclear

https://doi.org/10.1021/acs.inorgchem.2c00714
Inorg. Chem. 2022, 61, 8267−8282

Ru(II) complexes could exert their activities through different anticancer mechanisms and enabled near-infrared imaging.

EXPERIMENTAL SECTION

Materials and Measurements. All chemical reagents were purchased commercially and used directly without further purification unless specified. The solvents MeOH and EtOH were dried with CaH_2 and then distilled before use. *cis*-$Ru(bpy)_2Cl_2{\cdot}2H_2O$ was synthesized through the reported method.[33] ^1H and ^{13}C NMR spectra were recorded on a Bruker DRX-400 spectrometer. High-resolution electrospray ionization mass spectra (HRMS) were recorded using a 6224-TOF-LC/MS (Agilent). HaCat, HeLa, A549, and A549/DDP were purchased from Fenghui Biology Company. Cell uptake, cell cycle distribution, cell apoptosis, and ROS experiments were measured by flow cytometry (BD Accuri C6 Plus) and analyzed using FlowJo software. A UH4150 UV−vis recording spectrophotometer and an RF6000 spectrophotometer (SHIMADAZU) were used with 1 cm-path length quartz cuvettes (3 mL). Spectra were processed using Originlab software. Experiments were carried out at 298 K unless otherwise stated.

Synthesis of the Complex ***RuY.*** Under N_2, a Schlenk bottle containing *cis*-$Ru(bpy)_2Cl_2{\cdot}2H_2O$ (0.104 g, 0.2 mmol) and **YL-2** (0.039 g, 0.2 mmol) was treated with methanol (20 mL), and the mixture was refluxed for 6 h. The resulting red-brown solution was concentrated under reduced pressure to give a red-brown solid. The resulting solid was purified by flash column chromatography on neutral Al_2O_3 (200−300 mesh) (eluents: CH_2Cl_2/MeOH = 20:1) and then recrystallized by layering CH_2Cl_2 and MeOH with toluene ($V_{DCM}/V_{MeOH}/V_{tol}$ = 6:2:15) to give brown crystals (0.085 g, 66% yield). Mp: >260 °C. ^1H NMR (400 MHz, $CDCl_3$−CD_3OD) δ 8.77−8.63 (m, 2H), 8.55−8.48 (m, 1H), 8.42 (ddd, J = 8.3, 3.5, 2.3 Hz, 2H), 8.05 (tdd, J = 7.9, 5.0, 1.5 Hz, 2H), 7.94 (td, J = 7.9, 1.6 Hz, 1H), 7.87−7.74 (m, 4H), 7.70−7.60 (m, 3H), 7.43−7.32 (m, 3H), 7.25−7.21 (m, 1H), 7.18 (ddd, J = 7.2, 5.7, 1.3 Hz, 1H), 7.10 (ddd, J = 7.3, 5.7, 1.5 Hz, 1H), 7.02 (ddd, J = 8.2, 7.0, 1.1 Hz, 1H), 6.69 (ddd, J = 8.3, 7.0, 1.2 Hz, 1H), 5.52 (d, J = 8.0 Hz, 1H). ^{13}C NMR (101 MHz, $CDCl_3$−CD_3OD) δ 158.55, 158.29, 158.04, 157.27, 157.22, 155.47, 151.75, 151.53, 150.95, 150.88, 149.84, 146.92, 144.67, 137.38, 137.34, 136.89, 136.80, 136.19, 127.69, 127.15, 127.12, 126.65, 124.78, 124.52, 124.28, 123.77, 123.67, 122.48, 121.85, 121.44, 119.22, 113.08. HRMS: Calcd for $C_{32}H_{24}N_7Ru^+$ $[M - Cl^-]^+$: 608.1131. Found: 608.11316.

Synthesis of the Complex ***RuY1.*** Under N_2, a Schlenk bottle containing *cis*-$Ru(bpy)_2Cl_2{\cdot}2H_2O$ (0.370 g, 0.55 mmol) and **YL-1** (0.181 g, 0.5 mmol) was treated with methanol (80 mL), and the mixture was refluxed for 24 h. The resulting red-brown solution was concentrated under reduced pressure to give a red-brown solid. The resulting solid was purified by flash column chromatography on neutral Al_2O_3 (200−300 mesh) (eluents: CH_2Cl_2/MeOH = 20:1) and then recrystallized by layering CH_2Cl_2 and MeOH with hexane and Et_2O ($V_{DCM}/V_{MeOH}/V_{hexane}/V_{ether}$ = 3:1:4:4) to give dark-brown crystals (0.34 g, 84% yield), which was suitable for single-crystal X-ray diffraction analysis. Mp: >260 °C. ^1H NMR (400 MHz, CD_3OD) δ 8.76−8.61 (m, 3H), 8.54 (td, J = 8.9, 1.9 Hz, 2H), 8.46 (dt, J = 5.6, 1.3 Hz, 1H), 8.26 (dt, J = 8.2, 1.1 Hz, 1H), 8.20 (dd, J = 4.7, 2.4 Hz, 1H), 8.12 (td, J = 7.9, 1.4 Hz, 1H), 8.08−7.95 (m, 3H), 7.85−7.76 (m, 2H), 7.74−7.64 (m, 2H), 7.38 (tdd, J = 7.2, 3.5, 2.0 Hz, 5H), 7.32 (ddt, J = 5.7, 1.7, 0.9 Hz, 1H), 7.18 (ddd, J = 7.2, 5.6, 1.4 Hz, 1H), 7.08 (ddd, J = 8.3, 7.0, 1.2 Hz, 1H), 6.98 (dd, J = 6.1, 2.6 Hz, 2H), 6.70 (ddd, J = 8.3, 7.0, 1.2 Hz, 1H), 5.54−5.40 (m, 1H). ^{13}C NMR (101 MHz, $CDCl_3$−CD_3OD) δ 160.00, 159.30, 158.11, 157.51, 156.64, 156.36, 153.81, 152.58, 152.10, 151.44, 150.95, 148.98, 147.41, 145.71, 138.84, 138.30, 136.50, 136.06, 135.93, 134.30, 127.41, 126.65, 126.27, 124.50, 123.52, 123.41, 122.79, 122.55, 122.40, 122.16, 121.01, 119.70, 113.72. HRMS: Calcd for $C_{42}H_{29}N_{10}Ru^+$ $[M - Cl]^+$: 775.1620. Found: 775.1606.

Synthesis of the Complex ***RuY2.*** Under N_2, a Schlenk bottle containing *cis*-$Ru(bpy)_2Cl_2{\cdot}2H_2O$ (0.016 g, 0.03 mmol), **RuY1** (0.023 g, 0.03 mmol), and *t*BuOK (0.014 g, 0.12 mmol) was treated with ethanol (15 mL), and the mixture was refluxed for 24 h. The resulting dark-purple solution was concentrated under reduced pressure to give a dark-purple solid. The resulting solid was purified by flash column chromatography on neutral Al_2O_3 (200−300 mesh) (eluents: CH_2Cl_2/MeOH = 20:1) and then recrystallized by layering CH_2Cl_2 and MeOH with hexane and Et_2O ($V_{DCM}/V_{MeOH}/V_{hexane}/V_{ether}$ = 3:1:4:4) to give black-purple crystals (0.031 g, 85% yield), which was suitable for single-crystal X-ray diffraction analysis. Mp: >260 °C. ^1H NMR (400 MHz, CD_3OD) δ 8.82−8.72 (m, 3H), 8.68 (dd, J = 8.3, 2.8 Hz, 1H), 8.62 (d, J = 8.2 Hz, 1H), 8.58−8.46 (m, 3H), 8.43 (d, J = 8.1 Hz, 1H), 8.23 (t, J = 8.5 Hz, 2H), 8.11 (dt, J = 14.4, 7.9 Hz, 2H), 8.02 (d, J = 5.4 Hz, 1H), 7.99−7.76 (m, 6H), 7.73−7.60 (m, 5H), 7.52 (q, J = 4.8, 4.2 Hz, 2H), 7.40−7.09 (m, 9H), 7.01 (dd, J = 12.2, 6.3 Hz, 2H), 6.92 (d, J = 2.1 Hz, 1H), 6.82 (td, J = 7.8, 3.3 Hz, 1H), 6.63 (t, J = 7.6 Hz, 1H), 5.86 (d, J = 8.2 Hz, 1H), 5.49 (d, J = 8.2 Hz, 1H). ^{13}C NMR (101 MHz, CD_3OD) δ 160.52, 159.34, 158.21, 158.00, 157.82, 157.41, 156.95, 156.27, 156.09, 155.08, 154.62, 153.26, 152.64, 152.00, 150.53, 150.27, 149.32, 146.85, 145.28, 143.36, 141.72, 136.30, 136.06, 135.29, 134.92, 134.68, 134.49, 134.03, 133.94, 126.62, 126.41, 126.22, 126.11, 125.82, 123.22, 123.18, 123.07, 122.99, 122.90, 122.41, 122.16, 121.98, 121.42, 121.21, 118.55, 118.35, 114.77, 114.39, 113.19. HRMS: Calcd for $C_{62}H_{44}N_{14}Ru_2^{2+}$ $[M - Cl + H]^{2+}$: 1188.1949. Found: 594.09821 (z = 2).

Log P_{ow} Determination. The log P_{ow} determination of complexes **RuY**, **RuY1**, and **RuY2** was conducted using the shake-flask method. **RuY**, **RuY1**, and **RuY2** (40 μM) were dissolved in double-distilled water, and the solution was filtered to remove undissolved ruthenium complexes. Subsequently, the solution was added to an equal volume of *n*-octanol (presaturated with water), shaken vigorously at 37 °C for 24 h, and centrifuged for 15 min to achieve phase separation. The initial and final concentrations of compounds in the aqueous phase were determined by the UV−vis spectrum method, and the water−octanol partition coefficients ($\log P_{ow}$) were calculated.

Fluorescence Quantum Yield. Quantum yields (QY) of complexes **RuY**, **RuY1**, and **RuY2** were measured using $Ru(bpy)_3^{2+}$ as a standard (λ_{ex} = 450 nm in MeCN, Φ = 0.018). The QY of complexes **RuY**, **RuY1**, and **RuY2** can be calculated from eq 1

$$\Phi_f^i = \frac{F^i f_s n_i^2}{F^s f_i n_s^2}\Phi_f^s \tag{1}$$

where Φ_f^i and Φ_f^s are the photoluminescence QY of the sample and that of the standard, respectively, F^i and F^s are the integrated intensities (areas) of the sample and standard spectra, respectively, f_x is the absorption factor (also known under "absorptance"), the fraction indices impinging on the sample that is absorbed ($f_x = 1 - 10^{-A_x}$, where A = absorbance), and n_i and n_s are the refractive indices of the sample and reference solution, respectively.[34]

Molecular Docking. The structures of the three complexes were sketched using SYBYL-X 2.1 software (Tripos Inc., St. Louis, MO), and the energy-minimized conformations were obtained with the Tripos force field. The docking studies of the molecules with calf thymus DNA (CT-DNA) were accomplished by docking these complexes into B-DNA. The crystal structure of B-DNA (PDB ID: 3IXN) was downloaded from the Protein Data Bank. Then, the docking studies were implemented with the Surflex-Dock Geom module in SYBYL-X 2.1. The visualization of the docking results was performed using PyMOL software (DeLano Scientific LLC, San Carlos, CA).

Electronic Absorption Titration Studies. DNA binding experiments were carried out in Tris-HCl buffer (5 mM Tris-HCl, 10 mM NaCl buffer solution, pH = 7.4) using DMSO solutions of complexes **RuY**, **RuY1**, and **RuY2** and then diluting them suitably with buffer to the required concentrations for all the complexes (**RuY**: 40 μM, **RuY1**: 25 μM, and **RuY2**: 20 μM). During the experiment, the concentration of the complexes was constant, and the same volume of CT-DNA solution was added to the reference solution and the test solution (ε_{260nm}, CT-DNA = 6600 M^{-1} cm^{-1} per nucleotide) to reduce the influence of the absorption of CT-DNA at 260 nm on the

https://doi.org/10.1021/acs.inorgchem.2c00714
Inorg. Chem. 2022, 61, 8267−8282

experiment. After each addition, samples were incubated under physiological conditions (5 mM Tris-HCl, 10 mM NaCl buffer solution, pH = 7.4) at room temperature for 5 min equilibration time, and then, the UV−visible spectra were recorded. Spectra were collected from 250 to 600 nm after successive addition of CT-DNA (0−93.3 μM) into a 6 mL solution of each complex. The absorbance (A) of the most red-shifted band of each investigated complex was recorded after successive additions of CT-DNA. Interactions of the complexes **RuY**, **RuY1**, and **RuY2** with DNA were fitted to the Benesi−Hildebrand equation (eq 2) to calculate the binding constants K_b.

$$\frac{[DNA]}{\varepsilon_a - \varepsilon_f} = \frac{[DNA]}{\varepsilon_b - \varepsilon_f} + \frac{1}{K_b(\varepsilon_b - \varepsilon_f)} \quad (2)$$

where [DNA] is the concentration of CT-DNA and the apparent absorption coefficient, ε_a, corresponds to $A/[Ru]$. ε_b and ε_f refer to the extinction coefficient of the complexes in their bound and free forms, respectively. The plot of $[DNA]/(\varepsilon_a - \varepsilon_f)$ versus [DNA] gives a straight line, and the binding constant K_b was calculated as the slope/intercept ratio.

Ethidium Bromide Displacement Experiments. The experiments were carried out by the addition of the complexes **RuY**, **RuY1**, and **RuY2** to the samples containing 100 μM CT-DNA (nucleotide) and 20 μM EB (ethidium bromide) in a Tris buffer solution (5 mM Tris-HCl, 10 mM NaCl buffer solution, pH = 7.4). For each sample, the concentration of CT-DNA and EB was constant, and a solution of different complexes **RuY**, **RuY1**, and **RuY2** (dissolved with DMSO) was added. After each addition, samples were incubated under physiological conditions (5 mM Tris-HCl, 10 mM NaCl buffer solution, pH = 7.4) at room temperature for 5 min equilibration time, and then, the fluorescence spectra were recorded. The influence of the addition of **RuY**, **RuY1**, and **RuY2** (0−50 μM) to the EB-DNA mixture was measured by recording the variations in the fluorescence emission spectra between 550 and 800 nm with an excitation at 537 nm.

Cell Culture. For cytotoxicity determination, four cell lines were used, HaCat (human immortal keratinocyte cell line), HeLa (human cervical carcinoma cell line), A549 (human non-small-cell lung cancer cell line), and A549/DDP (cisplatin-resistant non-small-cell lung cancer cell line), purchased from Fenghui Biology Company. Frozen HeLa cells were thawed out in a 25 cm^2 cell culture flask in DMEM (GIBCO/Invitrogen, Camarillo, CA) supplemented with 10% fetal bovine serum (FBS, Biological Industry, Kibbutz Beit Haemek, Israel) and 1% penicillin−streptomycin (100 U/mL penicillin and 10 μg/mL streptomycin, Solarbio Life Science, Beijing, China) and maintained at 37 °C in a 5% CO_2 atmosphere, replacing the medium twice a week. Frozen HaCat and A549 cells were thawed out in a 25 cm^2 cell culture flask in RPMI 1640 (GIBCO/Invitrogen, Camarillo, CA) supplemented with 10% fetal bovine serum (FBS, Biological Industry, Kibbutz Beit Haemek, Israel) and 1% penicillin−streptomycin (100 U/mL penicillin and 10 μg/mL streptomycin, Solarbio Life Science, Beijing, China) and maintained at 37 °C in a 5% CO_2 atmosphere, replacing the medium twice a week. Frozen A549/DDP cells were thawed out in a 25 cm^2 cell culture flask in F12K (Nanjing SenBeiJia Biological Technology Co., Ltd.) supplemented with 10% fetal bovine serum (FBS, Biological Industry, Kibbutz Beit Haemek, Israel) and 1% penicillin−streptomycin (100 U/mL penicillin and 10 μg/mL streptomycin, Solarbio Life Science, Beijing, China) and maintained at 37 °C in a 5% CO_2 atmosphere, replacing the medium twice a week.

ROS Generation. A549 cells were transplanted into 6-well plates with a density of 10^5/well and cultured at 37 °C in a 5% CO_2 atmosphere for 24 h. The complexes **RuY**, **RuY1**, and **RuY2** were dissolved in DMSO and diluted to 30 μM in medium (DMSO final concentration was 5%). Since the ROS level induced by aromatic-ruthenium complexes increased first and then decreased, the culture time was selected as 6 h for study. Then, reactive oxygen probe DCFH-DA (1 μL) was added and incubated at 37 °C for 20 min in darkness. A549 cells were washed with phosphate-buffered saline (PBS) three times and trypsinized. The fluorescence intensity of ROS in cells containing **RuY**, **RuY1**, and **RuY2** complexes was determined by flow cytometry (BD Accuri C6 Plus).

***In Vitro* Cytotoxicity.** The cytotoxic study was examined by 3-(4,5-dimethylthiazol-2-yl)-2,5-diphenyltetrazolium bromide (MTT) assay. The MTT proliferation assay is based on the reduction of the yellow MTT tetrazolium salt (3-[4,5-dimethylthiazol-2-yl]-2,5-diphenyltetrazolium bromide) by mitochondrial dehydrogenases to form a blue MTT formazan in viable cells. A total of 10^4 cells/wells were inoculated in 96-well plates and cultured in 100 μL of DMEM or RPMI 1640 or F12K medium containing 10% FBS and 1% double antibody at 37 °C with a 5% CO_2 atmosphere. The cells were grown for 24 h, and the growth medium was replaced with fresh medium containing different concentrations of the compounds to be assayed and maintained at 37 °C in a 5% CO_2 atmosphere for 72 h. Cisplatin was also tested as a positive control. After the treatment, cells were washed with phosphate-buffered saline (PBS) and incubated with fresh DMEM or RPMI 1640 or F12K medium containing MTT (5 mg/mL). The plates were incubated for 4 h, and 150 μL of DMSO was added to each well. The absorbance values of each well were measured at 490 nm with a Thermo Scientific microplate reader. The relative cell viability was calculated by the equation: cell viability (%) = (OD treated/OD control) × 100%. The IC_{50} values were calculated using SPSS software.

Cell Uptake. A549 cells were plated onto a 6-wells plate and incubated at 37 °C with a 5% CO_2 atmosphere for 24 h. The cells were treated with **RuY**, **RuY1**, and **RuY2** (20 μM) complexes for 24 h to evaluate the intracellular incorporation. After being washed with phosphate-buffered saline (PBS) three times, the A549 cells were trypsinized and collected. A flow cytometer (BD Accuri C6 Plus) was used for measuring the fluorescence intensity of cells containing complexes **RuY**, **RuY1**, and **RuY2**.

Mitochondrial Transmembrane Potential. A549 cells were planted in 35 mm glass-bottom culture dishes at a density of 1×10^4 and cultured overnight at 37 °C with a 5% CO_2 atmosphere overnight. After treating with 20 μM **RuY**, **RuY1**, and **RuY2** complexes for 6 h, cells were further stained using 1 μL of the mitochondrial membrane potential probe JC-1 for 30 min, followed by washing three times with PBS (pH = 7.4). Confocal fluorescence images were acquired on a Zeiss LSM 880 multiphoton laser scanning confocal microscope (Carl Zeiss, Germany) with a 20× water immersion objective (NA 1.0) using excitation wavelengths of 488 nm for JC-1. The signals of JC-1 aggregates were collected at 570−620 nm, and the signals of JC-1 monomers were collected at 493−620 nm.

A549 cells were transplanted into 6-well plates with a density of 10^5/well and cultured at 37 °C in a 5% CO_2 atmosphere for 24 h. The complexes **RuY**, **RuY1**, and **RuY2** were dissolved in DMSO and diluted to 20 μM in the medium. Then, the mitochondrial membrane potential probe JC-1 (0.5 μL) was added and incubated at 37 °C for 30 min in darkness. A549 cells were washed with phosphate-buffered saline (PBS) three times and trypsinized. The fluorescence intensity of JC-1 monomers in cells containing **RuY**, **RuY1**, and **RuY2** complexes was determined by flow cytometry (BD Accuri C6 Plus).

Mitochondrial DNA Damage Assay. A549 cells were transplanted into 6-well plates with a density of 10^5/well and cultured at 37 °C in a 5% CO_2 atmosphere for 24 h. The cells were treated with **RuY**, **RuY1**, and **RuY2** (20 μM) complexes for 6 h. After being washed with PBS three times, the A549 cells were trypsinized and collected. The PicoGreen concentrated solution is diluted with TE buffer in a ratio of 1:200 to prepare the PicoGreen dyeing working solution. The cells were resuspended with 150 μL of buffer, and then, an equal volume of PicoGreen staining working solution was added to mix them evenly. The reaction mixture was kept away from light and at room temperature for about 5−10 min. The fluorescence intensity of PicoGreen in cells containing **RuY**, **RuY1**, and **RuY2** complexes was determined by flow cytometry (BD Accuri C6 Plus). The excitation wavelength of the PicoGreen dye is 488 nm.

Cell Cycle Distribution. Flow cytometry analysis of the cell cycle of A549 cells caused by exposure to metal complexes was carried out using the cell cycle analysis kit (Yeasen Biotechnology, Shanghai, Co.,

https://doi.org/10.1021/acs.inorgchem.2c00714
Inorg. Chem. 2022, 61, 8267−8282

Scheme 1. (a, d) Schematic Presentation of the Synthesis of Ru(II) Complexes and (b, c) Molecular Structures of RuY1 and RuY2[a]

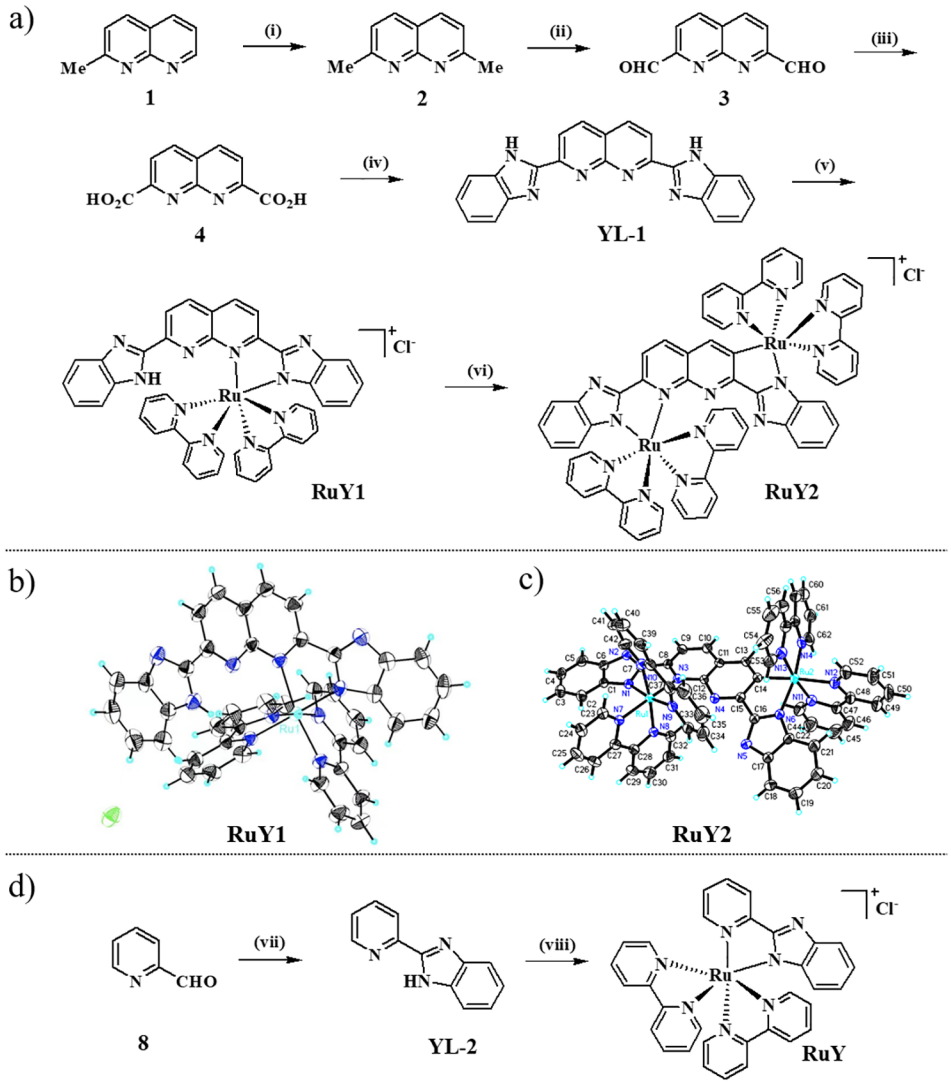

[a]Conditions: (i) a: MeLi, Et_2O, −78 °C, 4 h; b: $KMnO_4$, acetone, r.t., overnight, 80% total yield. (ii) SeO_2, dioxane, reflux 2 h, 73% yield. (iii) HNO_3, reflux 5 h, 78% yield. (iv) 1,2-Diaminobenzene, PPA, 220 °C, 5 h, 67% yield. (v) *cis*-$Ru(bpy)_2Cl_2{\cdot}2H_2O$ 1.1 equiv, MeOH, reflux 24 h, 84% yield. (vi) *cis*-$Ru(bpy)_2Cl_2{\cdot}2H_2O$ 1.0 equiv, *t*BuOK 4.0 equiv, EtOH, reflux 24 h, 85% yield. (vii) 1,2-Diaminobenzene, DMF/H_2O, 80 °C, 16 h, 81% yield. (viii) *cis*-$Ru(bpy)_2Cl_2{\cdot}2H_2O$ 1.0 equiv, MeOH, reflux 6 h, 66% yield.

Ltd.) according to the supplier's instructions. A549 cells were transferred into 6-well plates, with a density of 10^5/well, and cultured overnight at 37 °C in a 5% CO_2 atmosphere. Then, complexes **RuY**, **RuY1**, and **RuY2** were dissolved in DMSO (1 mM) and diluted with medium to 20 μM (the final concentration of DMSO was 1%) and cultured at 37 °C with a 5% CO_2 atmosphere for 24 h. As for the negative control, the same volume of DMSO was added. All adherent and floating cells were collected and washed twice with phosphate-buffered saline. After being centrifuged, 500 μL of staining solution, 5 μL of PI solution, and 10 μL of RNase A solution were added successively and dyed at 37 °C for 0.5 h under dark conditions. Cell pellets were washed and resuspended in PBS before being analyzed in a flow cytometer (BD Accuri C6 Plus) using excitation of DNA-bound PI at 488 nm, with emission at 585 nm. Data were processed using FlowJo software. The cell cycle distribution is shown as the percentage of cells containing G0/G1, S, G2/M-phase DNA as identified by propidium iodide staining.

Confocal Imaging. A549 cells were planted in 35 mm glass-bottom culture dishes at a density of 1×10^4 and cultured overnight at 37 °C in a 5% CO_2 atmosphere overnight. After treating with 20 μM **RuY**, **RuY1**, and **RuY2** complexes for 4 and 8 h, cells were further stained using 1 μL of Hoechst 33342 for 15 min, 0.1 μL of MitoTracker Green, and 1 μL of LysoTracker Green for 30 min, followed by washing three times with PBS (pH = 7.4). Confocal fluorescence images were acquired on a Zeiss LSM 880 multiphoton laser scanning confocal microscope (Carl Zeiss, Germany) with a 63× water immersion objective (NA 2.0) using excitation wavelengths of 405 nm for Hoechst 33342, 488 nm for LysoTracker Green and MitoTracker Green, and 514 nm for complexes **RuY**, **RuY1**, and **RuY2**. The signals of Hoechst 33342 were collected at 410−500 nm, the signals of MitoTracker Green and LysoTracker Green were collected at 493−620 nm, and the signals of **RuY**, **RuY1**, and **RuY2** were collected at 600−758 nm.

Apoptosis Study. Flow cytometry analysis of apoptotic populations of A549 and A549/DDP cells caused by exposure to metal complexes was carried out using the annexin V-FITC apoptosis detection kit (Yeasen Biotechnology, Shanghai, Co., Ltd.) according to the supplier's instructions. A549 and A549/DDP cells were

https://doi.org/10.1021/acs.inorgchem.2c00714
Inorg. Chem. 2022, 61, 8267−8282

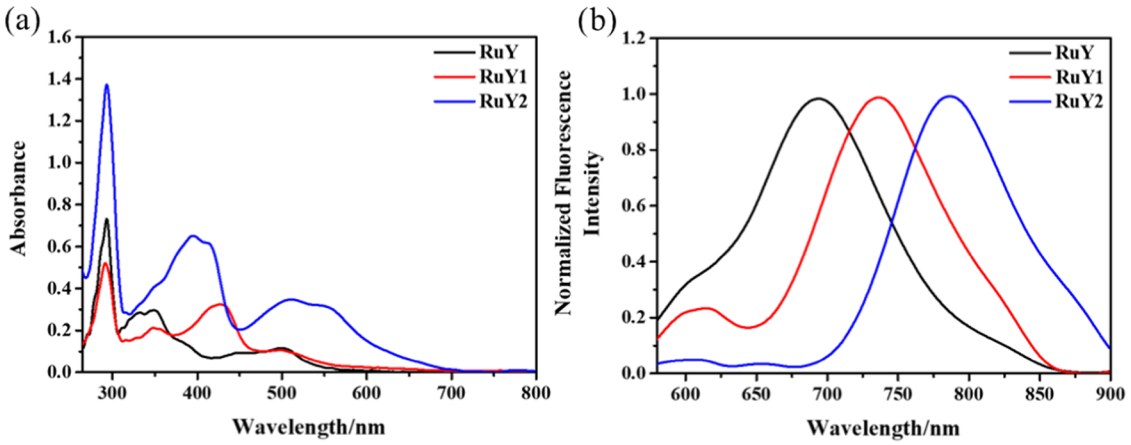

Figure 3. (a) UV−visible absorbance spectra of **RuY**, **RuY1**, and **RuY2** (10 μM) in DCM. (b) Normalized emission spectra of **RuY** (10 μM, λ_{ex} = 502 nm), **RuY1** (10 μM, λ_{ex} = 495 nm), and **RuY2** (10 μM, λ_{ex} = 509 nm) in DCM.

transferred into 6-well plates, with a density of 10^5/well, and cultured overnight at 37 °C in a 5% CO_2 atmosphere. Then, complexes **RuY**, **RuY1**, and **RuY2** were dissolved in DMSO (1 mM) and diluted with medium to 100 μM (the final concentration of DMSO was 5%) and cultured at 37 °C in a 5% CO_2 atmosphere for 24 h. As for the negative control, the same volume of DMSO was added. After digestion with trypsin without EDTA, all adherent and floating cells were collected and washed twice with phosphate-buffered saline. After being centrifuged, 500 μL of binding buffer, 5 μL of annexin V-FITC, and 10 μL PI staining solution were added successively and dyed at room temperature for 10−15 min under dark conditions. The samples were analyzed using a flow cytometer (BD Accuri C6 Plus).

RESULTS AND DISCUSSION

Synthesis and Characterization. The synthetic procedure is shown in Scheme 1. Starting from the commercial compound 2-methylnaphthyridine (**1**), the methylation gave 2,7-dimethyl-naphthyridine (**2**) in 80% isolated yield. Intermediate **2** underwent two-step oxidation with SeO_2 and nitric acid as the oxidants, respectively, giving the diacid product **4**. The condensation of diacid **4** with *o*-phenylenediamine in polyphosphoric acid (PPA) produced the desired tetradentate ligand 2,7-bis(1*H*-benzo[*d*]imidazol-2-yl)-1,8-naphthyridine **YL-1** in 67% isolated yield. The reaction of **YL-1** with 1.1 equiv of the Ru precursor *cis*-Ru(bpy)$_2$Cl$_2$·2H$_2$O in methanol under refluxing conditions afforded mononuclear **RuY1** in 84% isolated yield as a dark-brown crystal, which was obtained through recrystallization in the mixture of CH_2Cl_2, MeOH, hexane, and Et_2O. The molecular structure of **RuY1** was confirmed through single-crystal X-ray diffraction, as shown in Scheme 1b. It was found that the Ru center had been coordinated to two bipyridines and a pyridyl and a benzimidazolyl group to yield a regular octahedral geometry. Moreover, the formation of a covalent bond between the Ru center and N atom of the benzimidazolyl group made the Ru center a cation with a positive charge, and the corresponding anion was Cl^-. This kind of ionic structure led to water solubility, which is beneficial for applying as a bioactive molecule. The reaction of **YL-1** with 2.0 equiv of the Ru precursor *cis*-Ru(bpy)$_2$Cl$_2$·2H$_2$O was also investigated, but equally, mononuclear **RuY1** was obtained, and we failed to obtain a dinuclear Ru complex owing to the considerable steric hindrance between two benzimidazolyl groups and several bipyridines. Unexpectedly, when the reaction mixture of the mononuclear **RuY1** with *cis*-Ru(bpy)$_2$Cl$_2$·2H$_2$O had been treated with 4.0 equiv of *t*BuOK, dinuclear **RuY2** was successfully prepared in 85% isolated yield as a dark-purple crystal, which was analyzed through single-crystal X-ray diffraction, as shown in Scheme 1c. It was found from the molecular structure of the complex **RuY2** that the second Ru center was coordinated to not the N4 atom of naphthyridine but the C14 atom and similar to the **RuY1** center with a regular octahedral geometry. The dinuclear **RuY2** was also an ionic complex with a Cl^- as the anion. In addition, as a control trial, **RuY** bearing pyridyl benzimidazole **YL-2** was synthesized through the reaction of *cis*-Ru(bpy)$_2$Cl$_2$·2H$_2$O with the ligand pyridyl benzimidazole **YL-2**, which was obtained by a condensation reaction of pyridine-2-aldehyde (**5**) with *o*-phenylenediamine, as shown in Scheme 1d.

Photophysical Properties. The ground-state absorption spectra of Ru(II) polypyridyl complexes were characterized by strong absorption bands at ∼294 nm (**RuY** was ε = 77 440 M^{-1} cm^{-1}, **RuY1** was ε = 56 680 M^{-1} cm^{-1}, and **RuY2** was ε = 147 820 M^{-1} cm^{-1}), which was attributed to $\pi-\pi^*$ electronic transitions centered on aromatic rings, such as the 1,10-phenanthroline moiety, bipyrimidine, and the benzimidazole unit. A broad and intense band between 330 and 420 nm was due to an intra-ligand charge transfer (ILCT) transition.[35] This result could be confirmed by **YL-1** since **YL-1** also displayed an intense absorption at 394 nm (Figure S1). A broad band that was found in the 450−600 nm range corresponded to dp (Ru II)-π^*-metal-to-ligand charge-transfer (MLCT) transitions. Compared to the mononuclear Ru(II) complex **RuY1**, the absorption band of the dinuclear **RuY2** complex was shifted to a longer wavelength and became broader. In the meanwhile, the solvatochromism effect was observed when Ru(II) complexes were dissolved in the following solvents with increasing polarity: dichloromethane (DCM), chloroform ($CHCl_3$), acetonitrile (ACN), and methanol (MeOH). The absorption spectra (displayed in Figure S2 and Table S1) of **RuY2** consist of broad bands centered at 509, 508, 506, and 495 nm in DCM, $CHCl_3$, ACN, and MeOH, respectively. The other two complexes, **RuY** and **RuY1**, showed the same hypsochromic shift.

Luminescence was observed for both the ligand and its Ru(II) complexes in solution and at room temperature. Strong red emission bands were found at 696 nm for **RuY**, 740 nm for **RuY1**, and 786 nm for **RuY2**. These results fully proved that with the increase of ligand π-conjugation and the amount of

https://doi.org/10.1021/acs.inorgchem.2c00714
Inorg. Chem. 2022, 61, 8267−8282

Table 1. Fluorescence Characterization of RuY, RuY1, and RuY2

	λ_{abs} (nm)/ε (M^{-1} cm^{-1})	λ_{em} (nm)	QY[a]	log P_{ow}[b]	pK_a[c]
RuY	294 (77 440), 351 (29 670), 502 (11 640)	696	0.015	0.16 ± 0.20	6.4
RuY1	294 (56 680), 429 (32 350), 495 (10 830)	740	0.0037	−0.19 ± 0.01	
RuY2	294 (147 840), 396 (65 670), 509 (34 950)	786	0.0021	−0.85 ± 0.04	

[a]$Ru(bpy)_3^{2+}$ was used as a reference for quantum yield measurements (λ_{ex} = 450 nm). [b]Log P_{ow} of **RuY**, **RuY1**, and **RuY2** was determined by measuring the octanol/H_2O partition coefficients. [c]The pK_a value of **RuY**, **RuY1**, and **RuY2** obtained from the variation of the ratio of emission intensity at maximum versus pH (295 K, 5% DMSO in DI-water, **RuY**, λ_{ex} = 457 nm, **RuY1**, λ_{ex} = 477 nm, **RuY2**, λ_{ex} = 473 nm) (Figure S3).

Ru complexation, the spectrum was clearly red-shifted (Figure 3 and Table 1). Notably, **RuY1** and **RuY2** were completely unaffected by pH changes ranging from 2 to 13, while **RuY** had a pK_a of 6.4 (Figure S3). The stability of the three Ru(II) complexes in the biological medium (PBS buffer, 10% DMSO, pH = 7.4, incubation time = 24 h) has been checked by the emission intensity; the results showed good chemical stability (remained > 86%). Among them, **RuY2** was the most stable, and the stability order was **RuY2** (97.6%) > **RuY1** (96.4%) > **RuY** (86.0%) (Figure S4).

Docking Analysis. DNA is a key therapeutic target for metal anticancer drugs, and they may interact with DNA through covalent bonds, intercalation, groove binding, or electrostatic interactions. We first simulated the binding of our synthesized complexes to DNA by docking. The molecular docking method could offer a visual representation of the binding pattern of small ligands to DNA, which helps implement and verify the experimental results. As shown in Figure 4, the binding conformations of the dinuclear

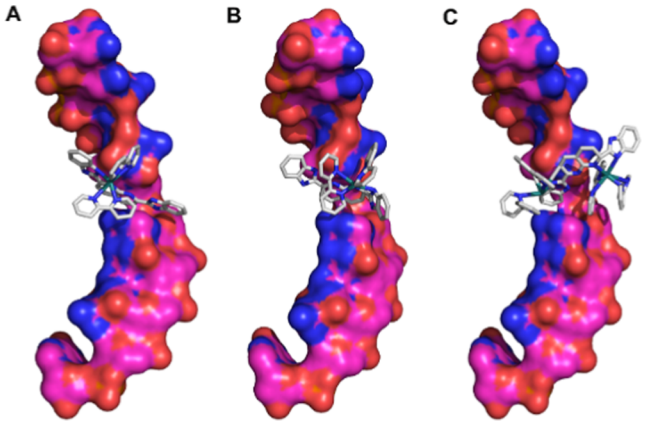

Figure 4. Docking results of complexes **RuY1** (A), **RuY** (B), and **RuY2** (C) into B-DNA (PDB ID: 3IXN).

ruthenium(II) complexes and DNA indicated that the complexes interacted with DNA mainly through the intercalations into the adjacent base pairs of the DNA. The backbones of the three complexes were inserted into the same space in varying degrees between the two bases: DT5 and DA6. In addition to the conventional interactions including van der Waals and hydrophobic interactions of the complexes with DNA, the pyridine rings of complexes **RuY1** and **RuY** and the phenyl ring of **RuY2** also formed $\pi-\pi$ stacking interactions with the surrounding bases. Also, this kind of intercalation could obviously increase the distance between the two adjacent bases. The calculated binding energies of **RuY**, **RuY1**, and **RuY2** were −17.12, −22.88, and −26.99 kJ/mol, respectively (Table S2). It suggested that complex **RuY2** is bound to DNA with the lowest binding energy.

Interaction with DNA. To confirm whether the simulation results of our docking analysis were correct, the UV−vis absorption spectrum and fluorescence spectrum were used to study the interaction of Ru(II) complexes with DNA. It has been reported that the Ru(II) complex can bind to DNA either by binding to the DNA groove or by partially intercalating into DNA. After binding to DNA, they exhibited a distinct bathochromic shift and hypochromisms in their visible absorption and UV bands. $\pi-\pi^*$ stacking occurs when the ligand from the complex is inserted between the DNA base pairs; then, the π^* empty orbital of the ligand is coupled with the π electron orbital of the base, resulting in a decrease in its energy level. Since the energy gap of the $\pi-\pi^*$ transition decreases, the UV absorption spectrum shows a bathochromic shift. At the same time, the coupled π orbitals are partially filled with electrons, reducing the probability of $\pi-\pi^*$ transitions, resulting in a hypochromatic effect.[36] The titration of our synthesized Ru(II) complexes with the calf thymus DNA (CT-DNA) was monitored by UV−vis spectra; the spectral behaviors of **RuY1** and **RuY2** were very similar, and they displayed obvious hypochromism, H% (as defined by $H\% \cong 100\ (A_{free} - A_{bound})/A_{free}$), and bathochromism, as indicated by $\Delta\lambda$ ($\Delta\lambda = \lambda_{bound} - \lambda_{free}$). Upon increasing concentrations of CT-DNA to the constant spectra (saturation), the H% ($\Delta\lambda$) values at ∼480 nm were found to be 45% (13 nm) and 37.5% (16 nm) for **RuY1** and **RuY2**, respectively. Thus, the evident spectral changes observed from **RuY1** and **RuY2** indicated a strong interaction between the complexes and the DNA, suggesting that these three molecules may bind to DNA in the form of partial insertion (Figure 5).

The values of the intrinsic DNA binding constant K_b were determined by monitoring the changes in absorbance at 286 nm with increasing DNA concentrations. The intrinsic DNA binding constants K_b obtained for **RuY**, **RuY1**, and **RuY2** were calculated to be 3.35×10^4, 2.20×10^4, and 4.73×10^4 M^{-1}, respectively. Among them, complex **RuY2** with DNA showed enhanced binding efficacy compared with that of complexes **RuY** and **RuY1**; this was probably because the two Ru(II) centers may not bind to the same double strands of the DNA strands (Table S3).

Changes in fluorescence spectra can be used to study the interaction between ruthenium complexes and DNA. The emission intensity of the Ru(II) complexes was affected by the hydrophobic environment of the base pair of the DNA. The vibrational mode of the complexes was restricted to some degree after binding with DNA. In the meanwhile, without the quenching of its fluorescence by water molecules, the fluorescence intensity of the complexes would be enhanced.[33] The responsive emission spectra of **RuY**, **RuY1**, and **RuY2** binding with DNA are shown in Figure 6. As can be seen from the figure, the fluorescence intensities of the solutions of the complexes **RuY**, **RuY1**, and **RuY2** increased significantly after the addition of CT-DNA, indicating that these three complexes

https://doi.org/10.1021/acs.inorgchem.2c00714
Inorg. Chem. 2022, 61, 8267−8282

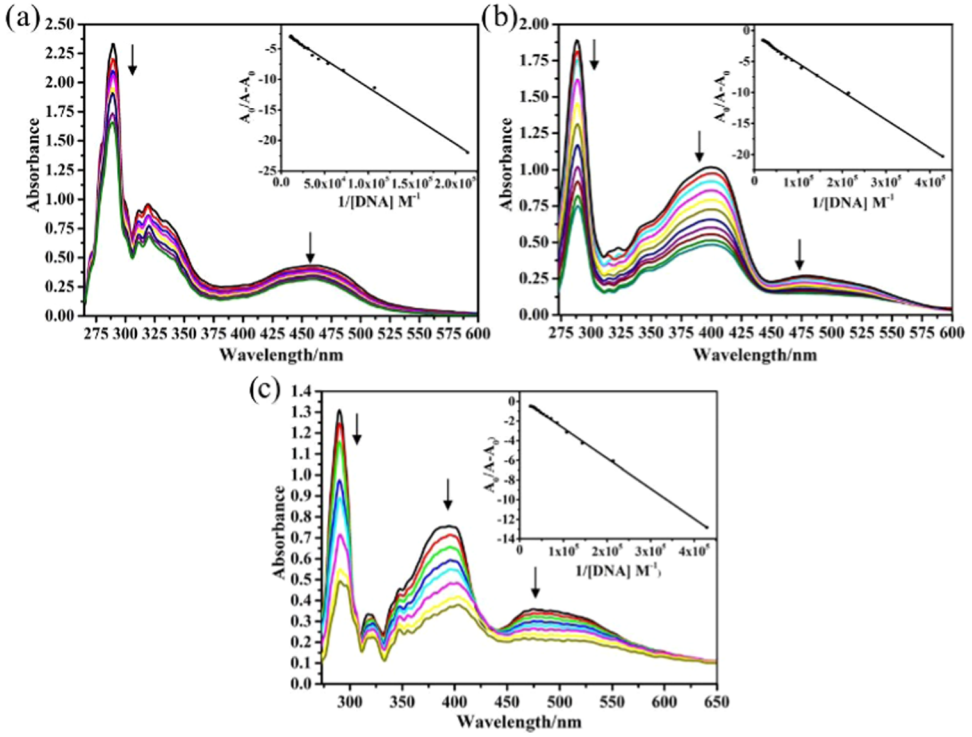

Figure 5. Absorption spectra of **RuY**, **RuY1**, and **RuY2** in Tris-HCl buffer upon addition of calf thymus DNA. (a) **RuY**: [Ru] = 40 μM, [DNA] = 0−93.3 μM; (b) **RuY1**: [Ru] = 25 μM, [DNA] = 0−51.3 μM, (c) **RuY2**: [Ru] = 20 μM, [DNA] = 0−42 μM. The arrow shows a decrease in absorption upon increasing DNA concentration.

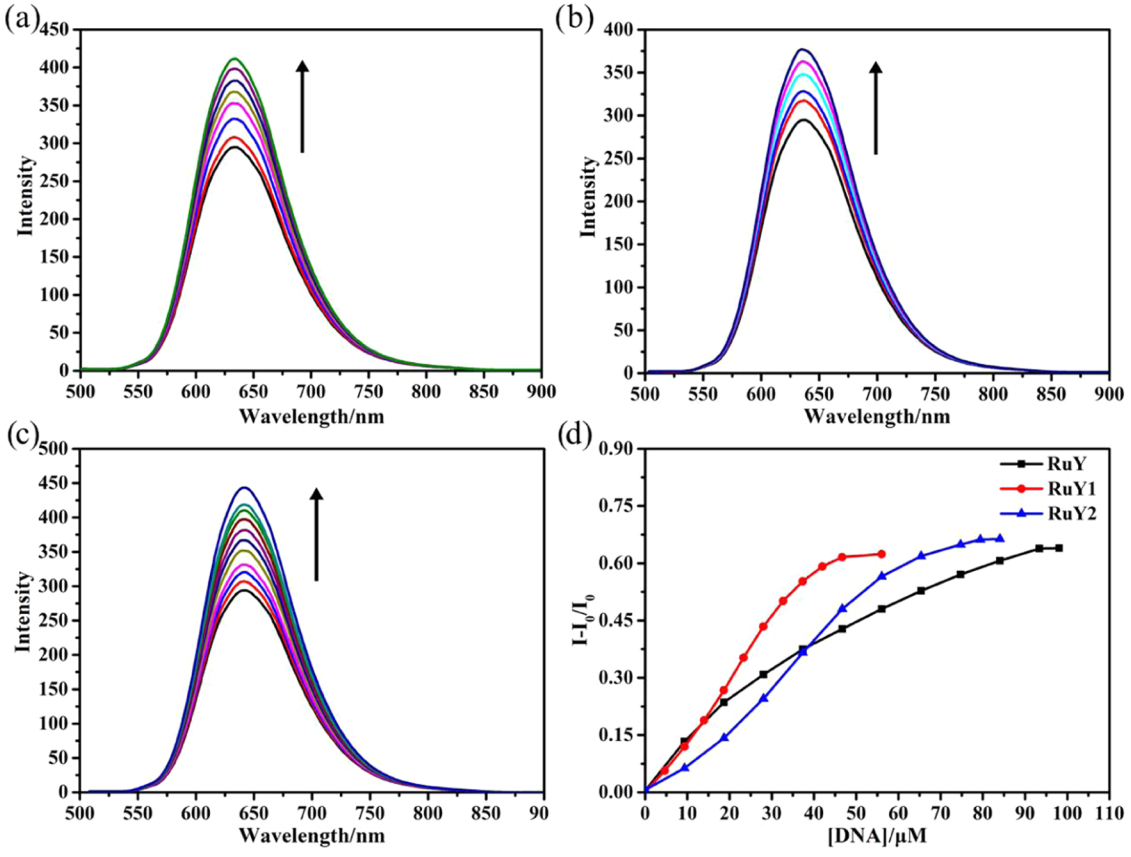

Figure 6. Emission spectra of **RuY** (a), **RuY1** (b), and **RuY2** (c) in the absence and the presence of increasing concentrations of DNA. ((d) **RuY**: [Ru] = 40 μM, [DNA] = 0−98.07 μM; **RuY1**: [Ru] = 25 μM, [DNA] = 0−46.67 μM, **RuY2**: [Ru] = 20 μM, [DNA] = 0−84.06 μM).

https://doi.org/10.1021/acs.inorgchem.2c00714
Inorg. Chem. 2022, 61, 8267−8282

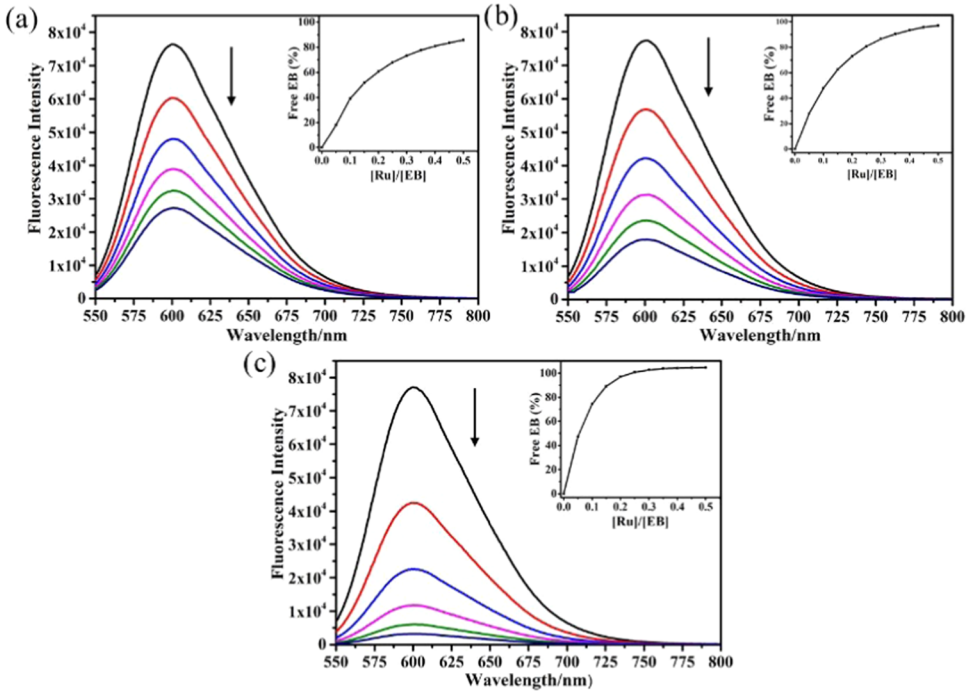

Figure 7. Fluorescence quenching curves of EB bound to DNA in the presence of complexes **RuY** (a), **RuY1** (b), and **RuY2** (c). [DNA] = 100 μM, [EB] = 20 μM, and [Ru] = 0−50 μM. The arrow shows a decrease in absorption upon increasing DNA concentration.

might interact with DNA. The fluorescence intensities of the complexes **RuY**, **RuY1**, and **RuY2** increased by 64.5, 63.9, and 66.0%, respectively, at their emission maximum.

Ethidium Bromide Displacement Experiments. Ethidium bromide (EB) can be a competitive binding agent for CT-DNA and complexes. The fluorescence of EB will be greatly enhanced after binding with CT-DNA. Thus, if the complexes can bind to CT-DNA in the insertion mode, they will compete with EB for the binding site, which leads to the fluorescence quenching of EB. The EB displacement experiment was conducted by adding complexes **RuY**, **RuY1**, and **RuY2** to the EB-DNA system (Figure 7). With the increase of the complexes' concentration, the fluorescence of the EB-DNA system displayed a gradual downward trend, with the decreasing amplitude reaching 89.9% (**RuY**), 98.6% (**RuY1**), and 99.6% (**RuY2**). Notably, the fluorescence intensity of the DNA-EB complex was reduced more remarkably by complexes **RuY1** and **RuY2**, probably attributed to the intercalation effect of the 2,7-bisbenzoimidazolyl-naphthyridine ligand. Although all three complexes have the same benzoimidazole and pyridine moieties, due to the complexation with ruthenium, **RuY1** and **RuY2** possess larger aromatic rings, which facilitated $\pi-\pi^*$ stacking; moreover, dinuclear Ru includes four bipyridyl ligands, which possess high potential to insert into the DNA ligand.[5] This result showed that the three complexes, **RuY**, **RuY1**, and **RuY2**, could replace EB from the EB-DNA system, indicating that these three Ru(II) complexes were likely to be bonded to CT-DNA through the insertion mode. Although groove binding reagents can also lower the fluorescence of the EB-DNA system, the general groove reagents decrease the fluorescence intensity of the system to a small extent.[37] The three complexes, **RuY**, **RuY1**, and **RuY2**, reduced the fluorescence intensity of the EB-DNA system by about 90%, indicating that the three Ru(II) complexes were bonded to CT-DNA in the intercalation mode.

ROS Generation. Ruthenium(II) arene complexes were reported to induce ROS production in cancer cells, which could be responsible for the cytotoxicity observed. Therefore, ROS levels in A549 cells induced by **RuY**, **RuY1**, and **RuY2** complexes were determined by flow cytometry. As shown in Figure 8, all three complexes significantly increased ROS levels in A549 cells, especially the dinuclear ruthenium(II) complex **RuY2**. Then, we quantified the results of flow cytometry, as

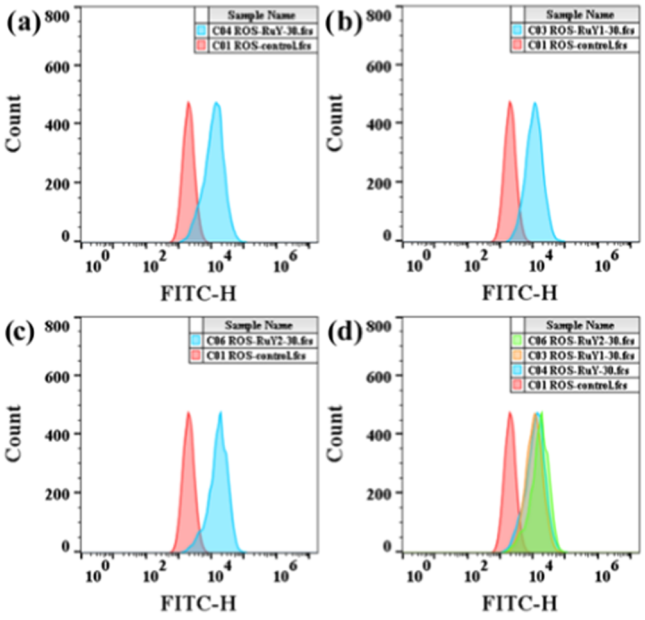

Figure 8. Analysis of ROS levels by flow cytometry after A549 cells were treated with complexes **RuY**, **RuY1**, and **RuY2** (30 μM) for 6 h and stained with DCFH-DA.

https://doi.org/10.1021/acs.inorgchem.2c00714
Inorg. Chem. 2022, 61, 8267−8282

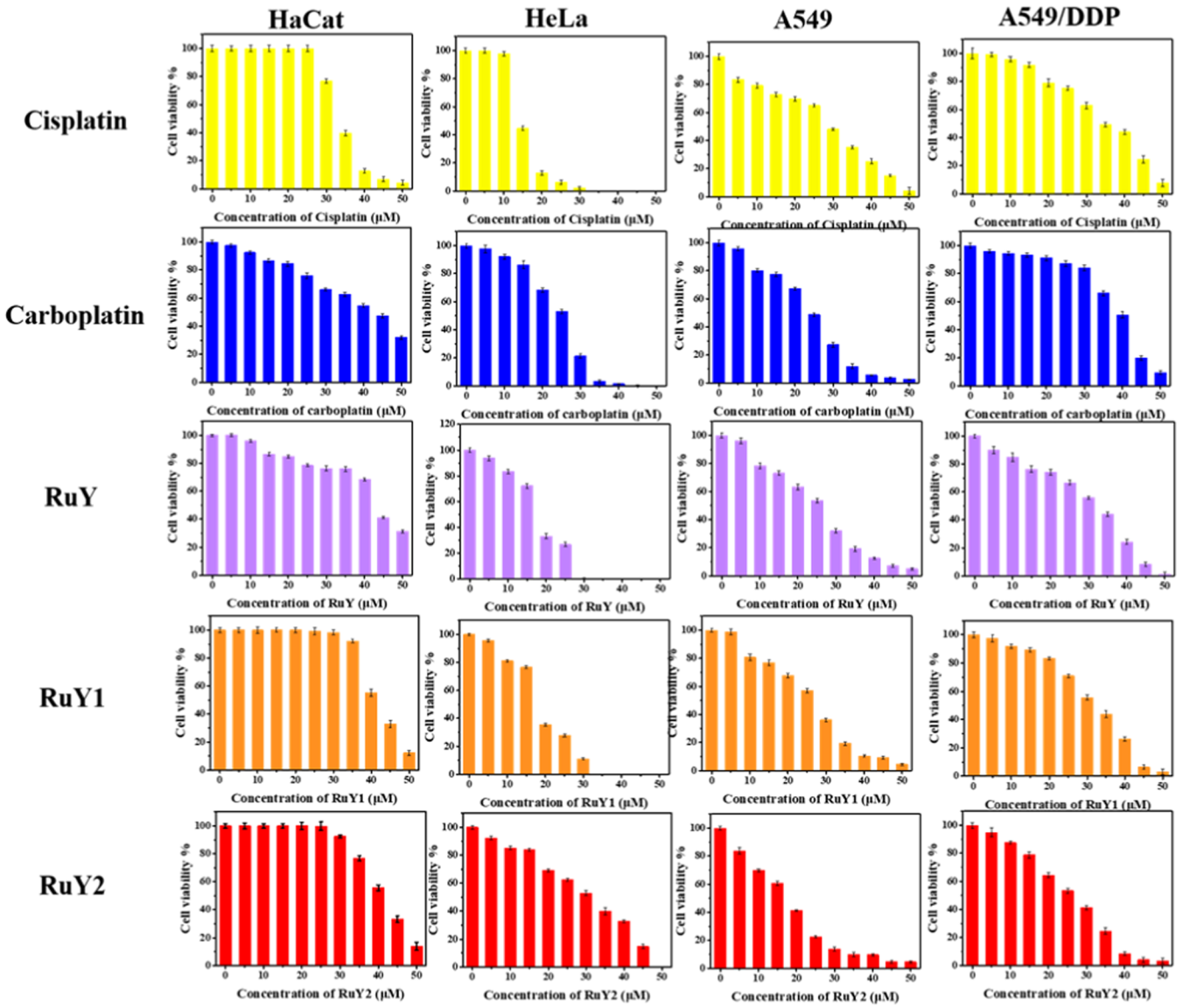

Figure 9. Cell survival rate of cisplatin, carboplatin, **RuY**, **RuY1**, and **RuY2** in HaCat, HeLa, A549, and A549/DDP cells incubated with the MTT method for 72 h.

shown in Figure S5. The relative order of ROS levels induced by these complexes is **RuY2** > **RuY** > **RuY1**.

***In Vitro* Cytotoxicity.** We evaluated the effects of cytotoxicity for Ru(II) polypyridyl complexes *in vitro* against the viability of HaCat (human keratinocyte cell line), HeLa (human cervical carcinoma cell line), A549 (human non-small-cell lung cancer cell line), and A549/DDP (cisplatin-resistant non-small-cell lung cancer cell line) by MTT assay after 72 h, and the concentrations were up to 50 μM (Figure 9). For comparison purposes, the cytotoxicity of cisplatin and carboplatin was also evaluated. The half-maximal inhibitory concentration (IC_{50}) values are listed in Table 2. Decreased cell viability is depicted in a dose-dependent manner in all four cell lines as a result of the MTT assay. Notably, **RuY2** exhibited better anticancer effects than those of cisplatin and carboplatin. The cytotoxicity of **RuY**, **RuY1**, and **RuY2** was lower than that of cisplatin and carboplatin in HaCat cells (normal cell) but was comparative in the HeLa cells. In terms of strong antiproliferative effects on the tested cancer cell lines, these ruthenium(II) complexes were further investigated to determine whether cisplatin resistance could be overcome. As shown in Table 2, the IC_{50} value of cisplatin against A549/DDP was increased to 43.0 μM, while the cytotoxicity of the complex against cisplatin-sensitive A549 and cisplatin-resistant A549/DDP cells was almost better. The cytotoxicity test of carboplatin followed the same trend. Especially, the IC_{50} of **RuY2** in the A549 cell line was 14.6 μM and in the A549/DDP

Table 2. *In Vitro* Cytotoxicity (IC_{50} μM) of RuY, RuY1, RuY2, Cisplatin, and Carboplatin against Human Cancer Cell Lines

	IC_{50} (μM)			
	HaCat	HeLa	A549	A549/DDP
RuY	44.8 ± 1.2	15.3 ± 1.0	21.3 ± 0.7	26.0 ± 1.1
RuY1	41.8 ± 0.3	10.0 ± 0.5	22.7 ± 0.4	29.1 ± 1.8
RuY2	40.8 ± 0.6	24.5 ± 1.6	14.6 ± 0.5	22.8 ± 0.7
cisplatin	34.0 ± 0.8	7.57 ± 0.3	22.3 ± 1.7	43.0 ± 1.1
carboplatin	39.8 ± 0.2	22.1 ± 0.6	20.0 ± 0.8	37.2 ± 0.8

https://doi.org/10.1021/acs.inorgchem.2c00714
Inorg. Chem. 2022, 61, 8267−8282

cell line was 22.8 μM, which indicated that these ruthenium(II) complexes could overcome cisplatin resistance.

Cell Uptake. Under the same experimental conditions, the cellular uptake of **RuY**, **RuY1**, and **RuY2** to A549 cells was evaluated by flow cytometry (Figure 10), and the flow

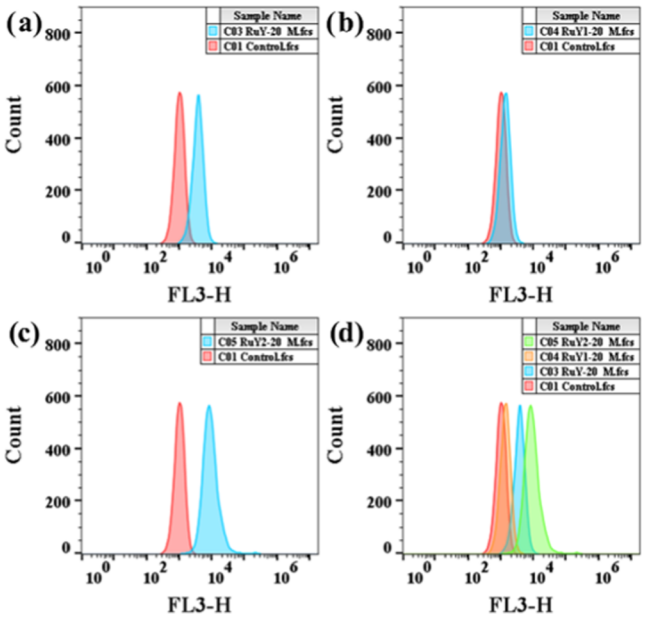

Figure 10. Flow cytometry of **RuY**, **RuY1**, and **RuY2** in the A549 cells (a), (b), (c), and control (d), dosed concentration = 20 μM and 24 h of incubation.

cytometric uptake was quantified, results of which are shown in Figure S6. The results show that **RuY2** has better uptake in A549 cells than that of **RuY** and **RuY1**. This is probably due to amphiphilic and cationic properties presenting better cell permeability.[38,39]

Mitochondrial Transmembrane Potential. JC-1 is a cationic lipid fluorescent dye, which has two states: monomer and polymer; their emission spectra are different. The membrane potential (Δy) of normal healthy mitochondria has polarity. JC-1 is rapidly absorbed into mitochondria depending on the polarity of Δy and forms a polymer in mitochondria due to the increase in concentration. The light emitted by the polymer is red fluorescence; when apoptosis occurs, the mitochondrial transmembrane potential is depolarized, and JC-1 is released from the mitochondria (the red light intensity decreases) and exists in the cytoplasm in the form of a monomer and emits green fluorescence. The results of confocal imaging (Figure 11) indicated that the complexes **RuY**, **RuY1**, and **RuY2** could reduce the mitochondrial membrane potential of A549 cells. The cells displayed red fluorescence when A549 cells were not treated with complexes **RuY**, **RuY1**, and **RuY2**, indicating that JC-1 existed in the form of aggregates, and the mitochondrial cell membrane was not damaged. All cells exhibited green fluorescence when the cells were treated with complexes **RuY**, **RuY1**, and **RuY2**, indicating that the mitochondrial cell membrane of A549 cells was damaged to varying degrees. JC-1 existed in the form of a monomer and showed green fluorescence, indicating that ROS produced by the complexes caused mitochondrial damage.

Similarly, we detected it by flow cytometry (Figure S7). The results displayed that compared with the control group, the fluorescence of the JC-1 monomer in the cells treated with the complex increased significantly and verified the damage of mitochondria. The figure on the right in Figure S7 is the quantization of the flow cytometry results, in which the decrease of the mitochondrial membrane potential caused by complex **RuY2** was the largest.

Mitochondrial DNA Damage Assay. PicoGreen is a fluorescent dye that detects double-stranded DNA. PicoGreen fluoresces only when bound to double-stranded DNA. It will not emit fluorescence when there is no DNA. The fluorescence intensity will decrease or disappear when double-stranded DNA is damaged or broken into single-stranded DNA. The results are shown in Figure 12a. Compared with the control, the fluorescence intensity of the complexes **RuY**, **RuY1**, and **RuY2** bound to PicoGreen all decreased, especially the complex **RuY2**. This result indicated that the complexes **RuY**, **RuY1**, and **RuY2** could insert into double-stranded DNA, disrupted DNA replication and transcription, and caused irreversible damage to mitochondrial DNA.

In addition, we further validated the experimental results by q-PCR, as shown in Figure 12b. The experimental results showed that the proportion of damaged mitochondrial DNA (mtDNA) to total mtDNA was significantly increased in the complexes **RuY**, **RuY1**, and **RuY2** compared to that in the control group, which indicated that the complexes **RuY**, **RuY1**, and **RuY2** were all capable of causing damage to mtDNA, with the complex **RuY2** causing the most severe damage. This was consistent with the results of the PicoGreen experiment and validates our experimental results.

Cell Cycle Distribution. The perturbation effects of cisplatin and Ru(II) polypyridyl complexes on the cell cycle progression of A549 cells were analyzed by flow cytometry (Figure 13). Most of the antineoplastic drugs in current use block the cell cycle in the S or G2/M phases.[40] Compared to the control, the cancer cells that were arrested at the S phase by our Ru(II) complexes were increased to 45.2% (**RuY**), 42.5% (**RuY2**), and 41.5% (**RuY1**) from 31.3% (control), which indicated that Ru(II) complexes affected the S phase more than other phases in A549 cells, which were similar to cisplatin.

Confocal Imaging. To this end, monitoring the microenvironment within defined subcellular organelles is important to help understand organelle-related pathophysiology. To investigate the cellular distribution, the subcellular localization of Ru(II) complexes was easily determined by confocal microscopy in A549 cells (Figure 14) and HeLa cells (Figures S8−S12) on account of their luminescence. To confirm their subcellular localization, costaining experiments using commercially available organelle-specific markers were performed. After 4 h of incubation with these complexes, the mitochondria-specific marker (Beyotime Biotechnology, Mito-Tracker Green, 5.0 μg/mL) was then added. The image in the right panel represented the merged image (yellow) of the Ru complex (left panel, red) with the MitoTracker (middle panel, green), clearly showing the colocalization of the Mitotracker with the complex in mitochondria. The results showed that all three Ru complexes targeted the mitochondria with high Pearson's colocalization coefficients (PCC) of 0.9502 (**RuY2**) in A549 cells and 0.9807 (**RuY2**) in HeLa cells after 4 h of incubation. The control experiment has been done with a commercially available lysosome tracker and nucleus tracker; minimal overlap was observed.

https://doi.org/10.1021/acs.inorgchem.2c00714
Inorg. Chem. 2022, 61, 8267−8282

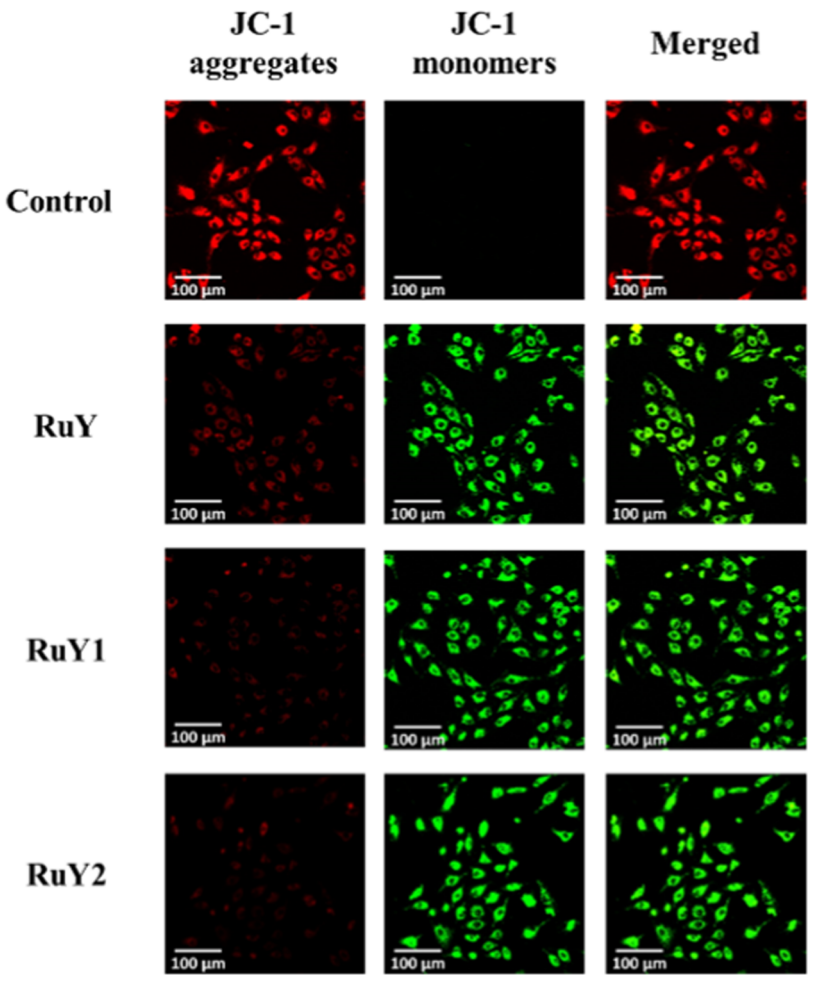

Figure 11. Confocal imaging of A549 cell membrane potential changes induced by complexes **RuY**, **RuY1**, and **RuY2** (20 μM, 6 h).

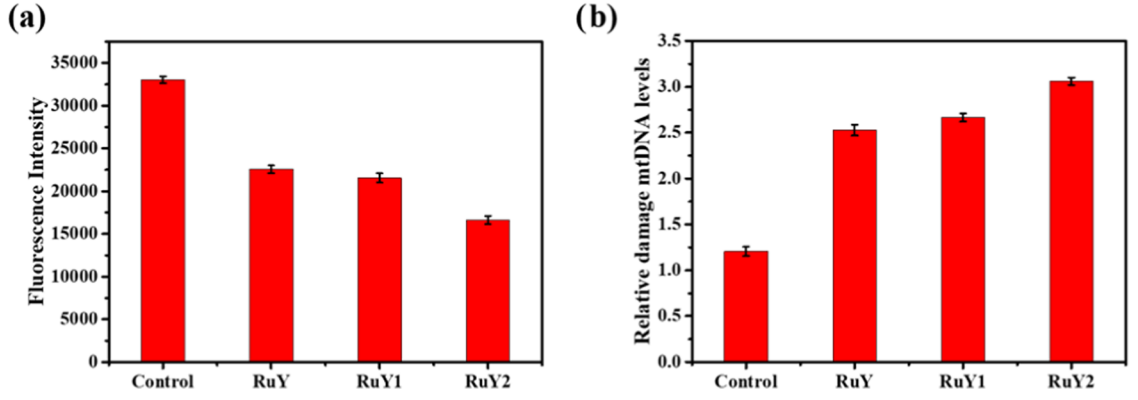

Figure 12. (a) PicoGreen staining experiment verified mitochondrial DNA damage caused by complexes **RuY**, **RuY1**, and **RuY2** (20 μM, 6 h). (b) q-PCR assay experiment verified mitochondrial DNA damage caused by complexes **RuY**, **RuY1**, and **RuY2** (20 μM, 6 h).

Apoptosis Study. The determination of the cellular death mechanism (necrosis or apoptosis) was performed using an annexin V-FITC/propidium iodide (PI) assay (Figure 15). Ru(II) complexes and cisplatin were incubated with A549 and A549/DDP cells for 72 h at a concentration of 50 μM. A549 and A549/DDP cells were treated with Ru(II) complexes, cisplatin, and negative control. The relative order of apoptosis induced against A549 cells was **RuY2** (33.9%) > **RuY** (30.1%) > cisplatin (28.7%) > **RuY1** (28.6%). The relative order of apoptosis induced against A549/DDP cells was **RuY2** (24.2%) > **RuY** (18.3%) > **RuY1** (12.5%) > cisplatin (5.52%), which was consistent with the result of the cytotoxicity study (Figure 9). According to the results, cell death was caused by apoptosis rather than necrosis, which proved that these Ru(II) polypyridyl complexes induce cell death through the apoptotic pathway.

CONCLUSIONS

In conclusion, three novel ruthenium(II) complexes, including mononuclear ruthenium complexes and dinuclear ruthenium

https://doi.org/10.1021/acs.inorgchem.2c00714
Inorg. Chem. 2022, 61, 8267−8282

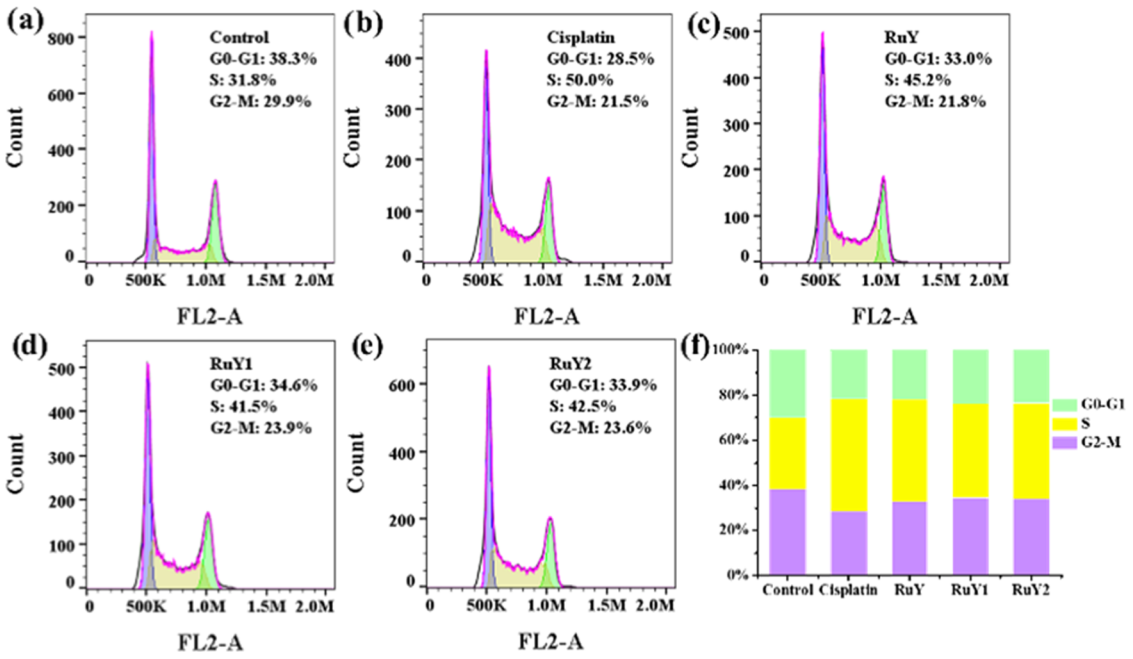

Figure 13. Cell cycle analysis of cell cycle distribution upon treatment with **RuY**, **RuY1**, and **RuY2** (20 μM) in A549 cells after 24 h of treatment. A selection of histograms show the strong effects of **RuY**, **RuY1**, and **RuY2** on cell cycle distribution. The DNA content of cells was analyzed by flow cytometry upon staining with propidium iodide and evaluated with FlowJo. Cisplatin was used as a positive control.

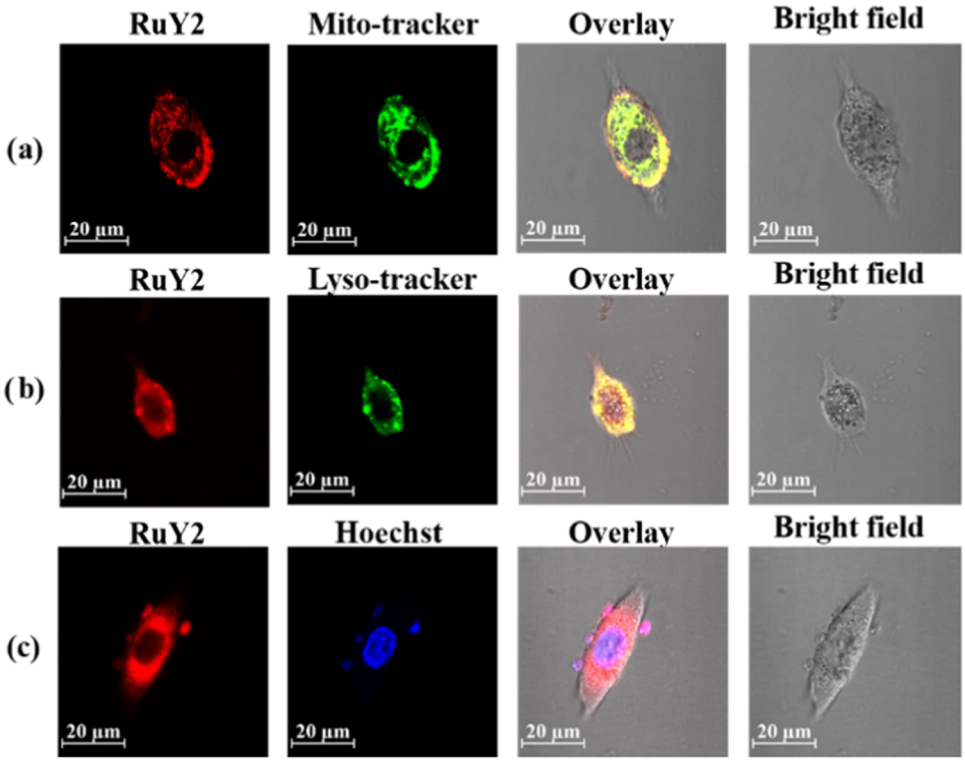

Figure 14. Subcellular localization of **RuY2** (20 μM, 4 h) in A549 cells was determined by confocal laser scanning microscopy. Colocalization images of A549 cells costained with **RuY2** and MitoTracker Green (a, 1 μL, 1 mM, 30 min), LysoTracker Green (b, 1 μL, 1 mM, 30 min), and Hoechst 33342 (c, 1 μL, 1 mM, 15 min). Scale bar: 20 μm.

complexes, were designed and synthesized. The photoluminescent tail of the dinuclear complex **RuY2** reached 900 nm, which is suitable for NIR imaging. *In vitro* experiments showed that the resulting ruthenium(II) complexes exhibited good antiproliferative activity against the tested cancer cells, while the cytotoxicity of the complex **RuY2** was superior to that of cisplatin. Further experimental and computational studies revealed that **RuY2** had a binding constant of about 4.73×10^4 M^{-1} for DNA, mainly through intercalation interactions. Furthermore, the three complexes could generate significant levels of ROS and further induce apotheosis. Therefore, we propose that these ruthenium(II) complexes

https://doi.org/10.1021/acs.inorgchem.2c00714
Inorg. Chem. 2022, 61, 8267−8282

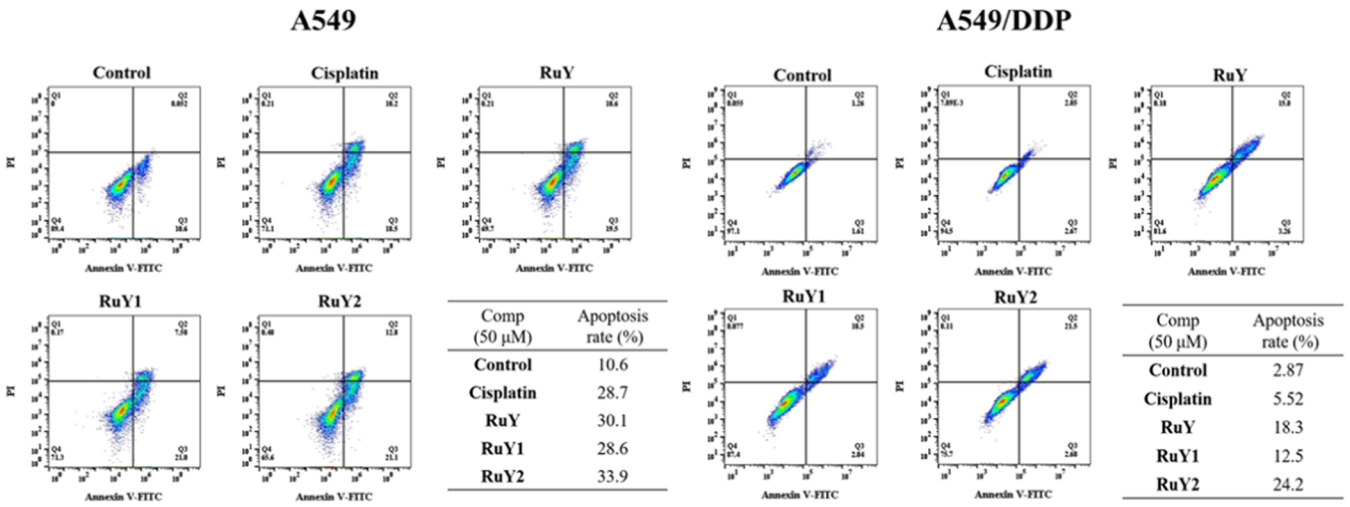

Comp (50 μM)	Apoptosis rate (%)
Control	10.6
Cisplatin	28.7
RuY	30.1
RuY1	28.6
RuY2	33.9

Comp (50 μM)	Apoptosis rate (%)
Control	2.87
Cisplatin	5.52
RuY	18.3
RuY1	12.5
RuY2	24.2

Figure 15. Flow cytometry analysis for apoptosis of A549 and A549/DDP cells induced by cisplatin and **RuY**, **RuY1**, and **RuY2** at the same concentration of 50 μM for 24 h. Lower left, living cells; lower right, early apoptotic cells; upper right, late apoptotic cells; and upper left, necrotic cells. The inserted numbers in the profiles indicate the percentage of the cells present in this area.

induced cell death through DNA binding and ROS-mediated apoptosis pathways, and the results of this study helped to reveal the mechanism of action of ruthenium(II) complexes. All three Ru(II) complexes could cross the cell membrane and were located in the mitochondria. Notably, the complex **RuY2** does not have cross-resistance with cisplatin due to different mechanisms of action. Overall, this dinuclear ruthenium(II) complex had unique biological properties and was a promising model for novel anticancer drug development.

■ ASSOCIATED CONTENT

Supporting Information

The Supporting Information is available free of charge at https://pubs.acs.org/doi/10.1021/acs.inorgchem.2c00714.

Experimental details, additional spectroscopic information, and biological supplementary data (PDF)

Accession Codes

CCDC 2130307 and 2130966 contain the supplementary crystallographic data for this paper. These data can be obtained free of charge via www.ccdc.cam.ac.uk/data_request/cif, or by emailing data_request@ccdc.cam.ac.uk, or by contacting The Cambridge Crystallographic Data Centre, 12 Union Road, Cambridge CB2 1EZ, UK; fax: +44 1223 336033.

■ AUTHOR INFORMATION

Corresponding Authors

Wenjing Ye − *Key Laboratory for the Synthesis and Application of Organic Functional Molecules, College of Chemistry and Chemical Engineering, Hubei University, Wuhan 430062, P. R. China; National & Local Joint Engineering Research Center of High-Throughput Drug Screening Technology, Hubei University, Wuhan 430062, P. R. China*; Email: wye@hubu.edu.cn

Jie Pan − *Key Laboratory for the Synthesis and Application of Organic Functional Molecules, College of Chemistry and Chemical Engineering, Hubei University, Wuhan 430062, P. R. China*; orcid.org/0000-0001-9245-0700; Email: j.pan@hubu.edu.cn

Authors

Jiaoyang Wang − *Key Laboratory for the Synthesis and Application of Organic Functional Molecules, College of Chemistry and Chemical Engineering, Hubei University, Wuhan 430062, P. R. China*

Yufei Zhang − *Key Laboratory for the Synthesis and Application of Organic Functional Molecules, College of Chemistry and Chemical Engineering, Hubei University, Wuhan 430062, P. R. China*

Yifan Li − *Key Laboratory for the Synthesis and Application of Organic Functional Molecules, College of Chemistry and Chemical Engineering, Hubei University, Wuhan 430062, P. R. China*

Enbo Li − *Key Laboratory for the Synthesis and Application of Organic Functional Molecules, College of Chemistry and Chemical Engineering, Hubei University, Wuhan 430062, P. R. China*

Complete contact information is available at: https://pubs.acs.org/10.1021/acs.inorgchem.2c00714

Notes

The authors declare no competing financial interest.

■ ACKNOWLEDGMENTS

This work was funded by grants from the National Natural Science Foundation of China [Nos. 22007029, 21502120].

■ REFERENCES

(1) Johnstone, T. C.; Suntharalingam, K.; Lippard, S. J. The next generation of platinum drugs: targeted Pt (II) agents, nanoparticle delivery, and Pt (IV) prodrugs. *Chem. Rev.* **2016**, *116*, 3436−3486.

(2) Rosenberg, B.; Vancamp, L.; Krigas, T. Inhibition of cell division in escherichia coli by electrolysis products from a platinum electrode. *Nature* **1965**, *205*, 698−699.

(3) Harrap, K. R. Preclinical studies identifying carboplatin as a viable cisplatin alternative. *Cancer Treat. Rev.* **1985**, *12*, 21−33.

(4) Cvitkovic, E.; Bekradda, M. Oxaliplatin: a new therapeutic option in colorectal cancer. *Semin. Oncol.* **1999**, *26*, 647−662.

(5) Zhao, J.; Li, S.; Wang, X.; Xu, G.; Gou, S. Dinuclear organoruthenium complexes exhibiting antiproliferative activity through DNA damage and a reactive-oxygen-species-mediated

endoplasmic reticulum stress pathway. *Inorg. Chem.* **2019**, *58*, 2208−2217.
(6) Liu, P.; Wu, B.; Liu, J.; Dai, Y.; Wang, Y.; Wang, K. DNA binding and photocleavage properties, cellular uptake and localization, and *in-vitro* cytotoxicity of dinuclear ruthenium (II) complexes with varying lengths in bridging alkyl linkers. *Inorg. Chem.* **2016**, *55*, 1412−1422.
(7) Adhireksan, Z.; Davey, G. E.; Campomanes, P.; Groessl, M.; Clavel, C. M.; Yu, H.; Nazarov, A. A.; Yeo, C. H. F.; Ang, W. H.; Droge, P.; Rothlisberger, U.; Dyson, P. J.; Davey, C. A. Ligand substitutions between ruthenium-cymene compounds can control protein versus DNA targeting and anticancer activity. *Nat. Commun.* **2014**, *5*, No. 3462.
(8) Soldevila-Barreda, J. J.; Romero-Canelon, I.; Habtemariam, A.; Sadler, P. J. Transfer hydrogenation catalysis in cells as a new approach to anticancer drug design. *Nat. Commun.* **2015**, *6*, No. 6582.
(9) Zhao, J.; Zhang, D.; Hua, W.; Li, W.; Xu, G.; Gou, S. Anticancer activity of bifunctional organometallic Ru (II) arene complexes containing a 7-hydroxycoumarin group. *Organometallics* **2018**, *37*, 441−447.
(10) Milutinović, M. M.; Čanović, P. P.; Stevanović, D.; Masnikosa, R.; Vraneš, M.; Tot, A.; Zarić, M. M.; Marković, B. S.; Marjanović, M. M.; Vučićević, L.; Savić, M.; Jakovljević, V.; Trajković, V.; Volarević, V.; Kanjevac, T.; Simović, A. R. Newly synthesized heteronuclear ruthenium (II)/ferrocene complexes suppress the growth of mammary carcinoma in 4T1-treated BALB/c mice by promoting activation of antitumor immunity. *Organometallics* **2018**, *37*, 4250−4266.
(11) Pan, J.; Jiang, L.; Chan, C.; Tsoi, T.; Shiu, K.; Kwong, D. W. J.; Wong, W.; Wong, W.; Wong, K. Excitation energy transfer in ruthenium (II)-porphyrin conjugates led to enhanced emission quantum yield and $^1O_2$ generation. *J. Lumin.* **2017**, *184*, 89−95.
(12) Brabec, V.; Kasparkova, J. Ruthenium coordination compounds of biological and biomedical significance. DNA binding agents. *Coord. Chem. Rev.* **2018**, *376*, 75−94.
(13) Bergamo, A.; Pelillo, C.; Chambery, A.; Sava, G. Influence of components of tumour microenvironment on the response of HCT-116 colorectal cancer to the ruthenium-based drug NAMI-A. *J. Inorg. Biochem.* **2017**, *168*, 90−97.
(14) Gransbury, G. K.; Kappen, P.; Glover, C. J.; Hughes, J. N.; Levina, A.; Lay, P. A.; Musgrave, I. F.; Harris, H. H. Comparison of KP1019 and NAMI-A in tumour-mimetic environments. *Metallomics* **2016**, *8*, 762−773.
(15) Bytzek, A. K.; Koellensperger, G.; Keppler, B. K.; Hartinger, C. G. Biodistribution of the novel anticancer drug sodium trans-[tetrachloridobis (1H-indazole) ruthenate (III)] KP-1339/IT139 in nude BALB/c mice and implications on its mode of action. *J. Inorg. Biochem.* **2016**, *160*, 250−255.
(16) Jose, D. A.; Sakla, R.; Sharma, N.; Gadiyaram, S.; Kaushik, R.; Ghosh, A. Sensing and bioimaging of the gaseous signaling molecule hydrogen sulfide by near-infrared fluorescent probes. *ACS Sens.* **2020**, *5*, 3365−3391.
(17) Zhang, J.; Ye, H.; Jin, Y.; Han, D. Recent Progress in Near-Infrared Organic Electroluminescent Materials. *Top. Curr. Chem.* **2022**, *380*, No. 6.
(18) Wu, C.; Mao, Y.; Wang, X.; Li, P.; Tang, B. Deep-tissue fluorescence imaging study of reactive oxygen species in a tumor microenvironment. *Anal. Chem.* **2022**, *94*, 165−176.
(19) Zhang, Y.; Wang, Y.; Song, J.; Qu, J.; Li, B.; Zhu, W.; Wong, W. Y. Near-infrared emitting materials via harvesting triplet excitons: molecular design, properties, and application in organic light emitting diodes. *Adv. Opt. Mater.* **2018**, *6*, No. 1800466.
(20) Wu, Y.; Wu, J.; Wong, W. Y. A new near-infrared phosphorescent iridium (III) complex conjugated to a xanthene dye for mitochondria-targeted photodynamic therapy. *Biomater. Sci.* **2021**, *9*, 4843−4853.
(21) Wu, J.; Li, Y.; Tan, C.; Wang, X.; Zhang, Y.; Song, J.; Qu, J.; Wong, W. Y. Aggregation-induced near-infrared emitting platinum (ii) terpyridyl complex: cellular characterisation and lysosome-specific localisation. *Chem. Commun.* **2018**, *54*, 11144−11147.
(22) Kloster, M. B. G.; Hannis, J. C.; Muddiman, D. C.; Farrell, N. Consequences of nucleic acid conformation on the binding of a trinuclear platinum drug. *Biochemistry* **1999**, *38*, 14731−14737.
(23) Haribabu, J.; Sabapathi, G.; Tamizh, M. M.; Balachandran, C.; Bhuvanesh, N. S. P.; Venuvanalingam, P.; Karvembu, R. Water-soluble mono- and binuclear Ru(*η*6-*p*-cymene) complexes containing indole thiosemicarbazones: synthesis, DFT modeling, biomolecular interactions, and *in vitro* anticancer activity through apoptosis. *Organometallics* **2018**, *37*, 1242−1257.
(24) Zeng, L.; Gupta, P.; Chen, Y.; Wang, E.; Ji, L.; Chao, H.; Chen, Z. The development of anticancer ruthenium (II) complexes: from single molecule compounds to nanomaterials. *Chem. Soc. Rev.* **2017**, *46*, 5771−5804.
(25) Baggaley, E.; Gill, M. R.; Green, N. H.; Turton, D.; Sazanovich, I. V.; Botchway, S. W.; Smythe, C.; Haycock, J. W.; Weinstein, J. A.; Thomas, J. A. Dinuclear ruthenium (II) complexes as two-photon, time-resolved emission microscopy probes for cellular DNA. *Angew. Chem., Int. Ed.* **2014**, *53*, 3367−3371.
(26) Liu, H.-Y.; Zhang, S.; Cui, M.; Gao, L.; Zhao, H.; Wang, K. pH-sensitive near-IR emitting dinuclear ruthenium complex for recognition, two-photon luminescent imaging, and subcellular localization of cancer cells. *ACS Appl. Bio Mater.* **2020**, *3*, 5420−5427.
(27) Raza, A.; Archer, S. A.; Fairbanks, S. D.; Smitten, K. L.; Botchway, S. W.; Thomas, J. A.; MacNeil, S.; Haycock, J. W. A dinuclear ruthenium (II) complex excited by near-infrared light through two-photon absorption induces phototoxicity deep within hypoxic regions of melanoma cancer spheroids. *J. Am. Chem. Soc.* **2020**, *142*, 4639−4647.
(28) Havrylyuk, D.; Heidary, D. K.; Nease, L.; Parkin, S.; Glazer, E. C. Photochemical properties and structure-activity relationships of Ru^{II} complexes with pyridylbenzazole ligands as promising anticancer agents. *Eur. J. Inorg. Chem.* **2017**, *2017*, 1687−1694.
(29) Yılmaz, I.; Akar, O. R.; Erkisa, M.; Selvi, S.; Şengül, A.; Ulukaya, E. Highly promising antitumor agent of a novel platinum (II) complex bearing a tetradentate chelating ligand. *ACS Med. Chem. Lett.* **2020**, *11*, 940−948.
(30) Yellol, G. S.; Donaire, A.; Yellol, J. G.; Vasylyeva, V.; Janiak, C.; Ruiz, J. On the antitumor properties of novel cyclometalated benzimidazole Ru (II), Ir (III) and Rh (III) complexes. *Chem. Commun.* **2013**, *49*, 11533−11535.
(31) Ye, W.; Zhao, M.; Du, W.; Jiang, Q.; Wu, K.; Wu, P.; Yu, Z. Highly Active Ruthenium (II) Complex Catalysts Bearing an Unsymmetrical NNN Ligand in the (Asymmetric) Transfer Hydrogenation of Ketones. *Chem. - Eur. J.* **2011**, *17*, 4737−4741.
(32) Four, M.; Riehl, D.; Mongin, O.; Blanchard-Desce, M.; Lawson-Daku, L. M.; Moreau, J.; Chauvin, J.; Delaire, J. A.; Lemercier, G. A novel ruthenium (II) complex for two-photon absorption-based optical power limiting in the near-IR range. *Phys. Chem. Chem. Phys.* **2011**, *13*, 17304−17312.
(33) Sullivan, B. P.; Salmon, D. J.; Meyer, T. J. Mixed phosphine 2, 2′-bipyridine complexes of ruthenium. *Inorg. Chem.* **1978**, *17*, 3334−3341.
(34) Brouwer, A. M. Standards for photoluminescence quantum yield measurements in solution. *Pure Appl. Chem.* **2011**, *83*, 2213−2228.
(35) Barton, J. K.; Danishefsky, A.; Goldberg, J. Tris-(phenanthroline)ruthenium (II): stereoselectivity in binding to DNA. *J. Am. Chem. Soc.* **1984**, *106*, 2172−2176.
(36) Hiort, C.; Lincoln, P.; Norden, B. DNA binding of.DELTA.-and.LAMBDA.-$[Ru(phen)_2DPPZ]^{2+}$. *J. Am. Chem. Soc.* **1993**, *115*, 3448−3454.
(37) Mardanya, S.; Karmakar, S.; Mondal, D.; Baitalik, S. Homo- and heterobimetallic rutheniumn (II) and osmium (II) complexes based on a pyrene-biimidazolate spacer as efficient DNA-binding probes in the near-infrared domain. *Inorg. Chem.* **2016**, *55*, 3475−3489.
(38) Singer, S. J.; Nicolson, G. L. The fluid nosaic model of the structure of cell membranes: cell membranes are viewed as two-dimensional solutions of oriented globular proteins and lipids. *Science* **1972**, *175*, 720−731.

https://doi.org/10.1021/acs.inorgchem.2c00714
Inorg. Chem. 2022, 61, 8267−8282

(39) Poon, C.-T.; Chan, P.; Man, C.; Jiang, F.; Wong, R. N. S.; Mak, N.; Kwong, D. W.; Tsao, S.; Wong, W. An amphiphilic ruthenium (II)-polypyridyl appended porphyrin as potential bifunctional two-photon tumor-imaging and photodynamic therapeutic agent. *J. Inorg. Biochem.* **2010**, *104*, 62−70.
(40) Gümüş, F.; Eren, G.; Acik, L.; Celebi, A.; Ozturk, F.; Yilmaz, S.; Sagkan, R. I.; Gur, S.; Ozkul, A.; Elmali, A.; Elerman, Y. Synthesis, cytotoxicity, and DNA interactions of new cisplatin analogues containing substituted benzimidazole ligands. *J. Med. Chem.* **2009**, *52*, 1345−1357.

https://doi.org/10.1021/acs.inorgchem.2c00714
Inorg. Chem. 2022, 61, 8267−8282